Journal of the American Heart Association

ORIGINAL RESEARCH

Interleukin 12p40 Deficiency Promotes Abdominal Aortic Aneurysm by Activating CCN2/MMP2 Pathways

Neekun Sharma, DVM, PhD; Chetan P. Hans, PhD

BACKGROUND: Development of abdominal aortic aneurysm (AAA) is associated with proinflammatory cytokines including interleukin-12 (IL12). Deficiency of interleukin 12p40 (IL12p40) increases localized fibrotic events by promoting TGFβ2 (transforming growth factor β)-dependent anti-inflammatory response. Here, we determined whether IL12p40 deficiency in apolipoprotein $E^{-/-}$ mice attenuates the development of AAA by antagonizing proinflammatory response.

METHODS AND RESULTS: Double knockout (DKO) mice were generated by crossbreeding $IL12p40^{-/-}$ mice with apolipoprotein $E^{-/-}$ mice (n=12). Aneurysmal studies were performed using angiotensin II (1 μg/kg/min; subcutaneous). Surprisingly, DKO mice did not prevent the development of AAA with angiotensin II infusion. Immunohistological analysis, however, showed distinct pathological features between apolipoprotein $E^{-/-}$ and DKO mice. Polymerase chain reaction (7 day) and cytokine arrays (28 day) of the aortic tissues from DKO mice showed significantly increased expression of cytokines related to anti-inflammatory response (interleukin 5 and interleukin 13), synthetic vascular smooth muscle cell phenotype (Activin receptor-like kinase-1 (ALK-1), artemin, and betacellulin) and T helper 17-associated response (4-1BB, interleukin-17e (Il17e) and Cd40 ligand (Cd-40L)). Indeed, DKO mice exhibited increased expression of the fibro-proteolytic pathway in the medial layer of aortae induced by cellular communication network factor 2 (CCN2) and $Cd3^{+}IL17^{+}$ cells compared with apolipoprotein $E^{-/-}$ mice. Laser capture microdissection showed predominant expression of CCN2/TGFβ2 in the medial layer of human AAA. Finally, *Ccn2* haploinsufficiency in the mice showed decreased AAA incidence in response to elastase infusion, associated with decreased matrix metalloproteinase-2 expression.

CONCLUSIONS: Our study reveals novel roles for *IL12p40* deficiency in inducing fibro-proteolytic activities in the aneurysmal mouse model. Mechanistically, these effects of IL12p40 deficiency are mediated by CCN2/matrix metalloproteinase-2 cross-talk in the medial layer of aneurysmal aortae.

Key Words: abdominal aortic aneurysm ■ CCN2 ■ IL12p40 ■ TGFβ2 ■ Th17

Abdominal aortic aneurysm (AAA) is a common vascular abnormality of the aorta with a prevalence of 9% to 13% in the elderly male population and 1% to 3% in the female population accounting for ≈150 000 to 200 000 deaths worldwide per year.[1] The majority of literature reports that proinflammatory myeloid cells are the key drivers for AAA pathogenesis.[2–6] However, approaches to limit the progression of small AAA (30–50 mm) using anti-inflammatory drugs in the clinical trials have not been successful.[7–9] Moreover, evidence suggests that aortic rupture is independent of inflammatory processes at the late stages of the disease.[10] Importantly, recent studies have suggested that anti-inflammatory interventions in AAA could be potentially harmful and need to be carefully monitored.[11–13] Studies in humans and mouse models of AAA have also identified the presence of anti-inflammatory macrophages, but there is

Correspondence to: Chetan P. Hans, PhD, School of Medicine-Cardiovascular Medicine & Medical Pharmacology and Physiology, University of Missouri, Rm: 324B Dalton Cardiovascular Research Center, 134 Research Park Drive, Columbia, MO 65211. E-mail: HansCP@health.missouri.edu

Supplementary Material for this article is available at https://www.ahajournals.org/doi/suppl/10.1161/JAHA.120.017633

For Sources of Funding and Disclosures, see page 17.

JAHA is available at: www.ahajournals.org/journal/jaha

CLINICAL PERSPECTIVE

What Is New?

- Deficiency of the proinflammatory cytokine interleukin 12p40 does not protect against abdominal aortic aneurysm in an angiotensin II-induced mouse model.
- Interleukin 12p40 deficiency enhances anti-inflammatory environment comprising increased TGFβ2 (transforming growth factor β2) and CCN2 (cellular communication network factor 2) expression.
- Global deficiency of interleukin 12p40 induces fibro-proteolytic events in the vascular smooth muscle cell-rich medial layer of the aorta.

What Are the Clinical Implications?

- Balance of pro- and anti-inflammatory macrophages, rather than predominance of either phenotype may be more relevant to alleviate abdominal aortic aneurysm burden.
- Inhibition of CCN2 signaling pathway may have translational implications because of its preventive effects on abdominal aortic aneurysm development.
- Further studies are warranted on the usage of anti-inflammatory interventions in patients with abdominal aortic aneurysm in the absence of overt proinflammatory environment.

Nonstandard Abbreviations and Acronyms

AngII	angiotensin II
CCN2	cellular communication network factor 2
DKO	double knockout
ECM	extracellular matrix
MMP	matrix metalloproteinase
qRT-PCR	quantitative reverse transcriptase polymerase chain reaction
TGFβ	transforming growth factor β
vSMC	vascular smooth muscle cell

no consensus on their exact roles in AAA.[5,9,14] These clinical observations warrant in-depth study on the role of anti-inflammatory factors, which may influence the development of AAA.

Distinct macrophage populations have both pathogenic and reparative roles in AAA depending upon the stages of the aneurysmal process. In response to a local vascular injury, naïve macrophages infiltrate and differentiate to induce a proinflammatory response associated with increased levels of interleukin-12 (IL12), iNOS, and low TGFβ2 (transforming growth factor β2) production.[15] IL12 is a potent proinflammatory cytokine principally expressed by macrophages and *IL12p40* deficient mice have a bias toward anti-inflammatory profile.[16] We recently demonstrated that global *IL12p40*-deficient mice (wild-type background) had increased TGFβ2-dependent fibrotic response in response to angiotensin II (AngII; a widely used model to induce AAA).[17] *IL12p40* deficiency in mice enhanced TGFβ2 and IL10 expression and reduced inflammatory responses. IL12 also antagonizes T helper (Th)2 responses by inhibiting IL4 production[18] and by negatively regulating natural regulatory T cells.[19,20]

TGFβ2 also plays a critical role in promoting structural and functional changes in the vascular smooth muscle cells (vSMCs) of the aortic medial layer.[21,22] During healthy conditions, contractile vSMCs in the medial layer maintain aortic wall integrity through biosynthesis of extracellular matrix (ECM).[23,24] In response to a vascular injury, contractile vSMCs undergo synthetic phenotypic changes and cell death by apoptosis.[25,26] The synthetic vSMCs are involved in the degradation of ECM through excessive production of matrix metalloproteinases (MMPs). Because of these features, phenotypic switching from contractile to synthetic vSMCs seems to be a key factor in the AAA formation.[27–29] Although, CCN2 (cellular communication network factor 2; previously known as CTGF)[30] and its upstream TGFβ2 signaling have been associated with synthetic modulation of vSMC,[31,32] their association with *IL12p40* deficiency and development of AAA are still poorly understood.

To examine the causative role of anti-inflammatory macrophages in AAA pathogenesis, we generated *IL12p40* deficient mice on *apoE*$^{-/-}$ background (double knockout; DKO mice) and performed aneurysmal studies using angiotensin II (AngII) infusion.[4,6,33] Surprisingly, we observed that DKO mice depicted increased fibrotic and proteolytic events, which can be attributed to 2 factors: (1) *IL12p40* deficiency significantly increased expression of CCN2/MMP2 in the medial layer of aorta; and (2) Increased CCN2/MMP2 is linearly correlated with medial vSMCs rather than adventitial fibroblasts in human AAA. We propose that AAA development in the DKO mice is primarily driven by crosstalk between anti-inflammatory macrophages/T cells and vSMCs.

METHODS

Study Approval

Mice were maintained in the Dalton Cardiovascular Research Center, and all procedures were performed

under a protocol approved by the Animal Care and Use Committee at the University of Missouri, Columbia and conform the National Institute of Health guidelines (*Guide for the Care and Use of Laboratory Animals*). We declare that the article adheres to the American Heart Association journals' implementation of the Animal Research: Reporting of In Vivo Experiments/Transparency and Openness Promotion Guidelines. The data that support the findings of this study are available from the corresponding author upon reasonable request. The details of the animals, cultured cells, and antibodies are listed in Data S1.

Animals and Aneurysmal Models

Eight-weeks old, *apoE*$^{-/-}$ (002052), *IL12p40*$^{-/-}$ (B6.129S1; 002693), and *Ccn2* haploinsufficient (*Ccn2*$^{+/-}$; 030769) mice were purchased from The Jackson Laboratory. The *apoE*$^{-/-}$ and *IL12p40*$^{-/-}$ mice were interbred to generate *IL12p40*$^{-/-}$*apoE*$^{-/-}$ (DKO) and the *apoE*$^{-/-}$ and DKO littermates were used for experiments. Similarly, *Ccn2*$^{+/-}$ male and females were interbred to generate *Ccn2*$^{+/+}$ and *Ccn2*$^{+/-}$ littermates and used for aneurysmal studies. Genotyping was performed according to The Jackson Laboratory's protocol. Male mice were used for these studies because of predominantly high incidence of AAA in these mice as detailed in the Arteriosclerosis, Thrombosis, and Vascular Biology Council statement.[34] Mice were kept on a 12 hours/12 hours light/dark cycle with standard chow. For AngII-induced aneurysmal studies, *apoE*$^{-/-}$ and DKO littermates (n=12) were infused with AngII (1 µg/kg/minute; Sigma) or saline for 28 days using published protocols.[4,6,17] In some experiments, *Ccn2*$^{+/+}$ and *Ccn2*$^{+/-}$ male littermate mice were infused with AngII (1 µg/kg/minute) for 7 days. Briefly, mice were anesthetized in a closed chamber with 1% to 2% isoflurane in oxygen for 2 to 5 minutes until immobile. Each mouse was then removed and taped on a heated (37°C±2°C) procedure board with 1.0±1.5% isoflurane administered via nosecone. Mini osmotic pumps (Alzet Model 2004) containing AngII or saline were implanted subcutaneously in the neck region of anesthetized mice per manufacturer's instructions. The mice were observed daily for sudden death throughout experimental duration. Mice found dead were immediately necropsied to determine the cause of death. After 28 days of treatment, the mice were euthanized using ketamine (150 mg/kg) and xylazine (20 mg/kg) and the aortae were dissected and processed accordingly for different assays.

For elastase model of aneurysm, AAA was induced as previously described.[35] Briefly, 8- to 10-week-old male *Ccn2*$^{+/+}$ and *Ccn2*$^{+/-}$ littermates (n=6) were anesthetized with an intraperitoneal injection of ketamine (100 mg/kg) and xylazine (5 mg/kg). Mice were administered buprenorphine (0.3 mg/kg) 1 hour before surgery for postoperative pain. For the elastase model, the animal was anesthetized with isoflurane (1%–2%; lack of response to toe pinch) and placed on a sterile surgical pad placed over a temperature-controlled heating pad. The abdominal aorta was isolated from the level of the left renal vein to the bifurcation and the branch of the abdominal aorta surrounding the site of distension was exposed and ligated with 10-0 sutures. Temporary 6.0-silk ligatures were placed around the proximal and distal portions of the aorta and an aortotomy was created at the bifurcation with a 30-gauge needle. Heat-tapered polyethylene tubing (PE-10) was introduced through the aortotomy and secured with a tie. Using a saline bag hung at the height of 136 cm to calibrate 100 mm Hg, the aorta was filled with the saline containing 4.5-U/mL type I porcine pancreatic elastase (Sigma). The aorta typically dilates to 150% to 170% of its original diameter during the 5- to 15-minute elastase perfusion. The control mice were infused with inactivated elastase. The perfusion catheter was removed thereafter and the aortotomy closed with a 10-0 suture to avoid constriction. After the aortotomy was closed, the distal and the proximal ligatures were removed. The wound was closed in 2 layers with 6-0 nylon/polypropylene suture; 0.25% bupivicaine drops or lidocaine (2%) (≈1 drop for each centimeter of the incision size) was placed on the wound. At the end of surgery, mice were placed on a temperature-controlled warming pad for recovery (about 15 minutes). The animals were allowed to recover in a clean cage and were monitored for at least 1 hour postoperatively. The mice were euthanized on day 14 of elastase treatment and the aortic diameter was measured.

Ultrasound Imaging of Mouse Aorta

Mice were restrained for <15 seconds to put into the anesthesia chamber, followed by anesthetization with oxygen and vaporized isoflurane (≈2%) as described.[17,36] Anesthesia was confirmed by loss of spinal reflexes via toe pinching, and the loss of corneal reflex by gentle touch of the eye with a soft tissue paper technique. The animals were placed on a heated (41°C) imaging stage in a supine position while under anesthesia. The body temperature, heart beat, and respiration rates were continuously monitored during the imaging procedure. The abdominal hairs were removed by applying Nair followed by cleaning with wet gauze. Warmed ultrasound gel was applied to the abdominal surface, and ultrasound probes applied to the gelled surface to collect B-mode, M-mode, ECG-based Kilohertz Visualization images

by the imaging system (Vevo 2100, VisualSonics) as described.[17,36]

Aortic Diameter Measurement

The AngII-induced AAAs were defined as having at least 50% increase in the maximal intraluminal and external diameters of the abdominal aorta compared with the control mice.[4,6] The maximal intraluminal diameter of the aortae was quantified in vivo by ultrasound imaging. For quantification of the maximal external aortic diameter, formalin fixed aortae were measured using ZEN lite software (Zen 2.3 blue edition; Zeiss, NY) ex vivo under a microscope. The average suprarenal aortic width was 0.87 mm in control mice, and consequently, we defined AAA as >1.31 mm.

Aortic Stiffness Measurement In Vivo and In Vitro

In vivo aortic stiffness was measured locally in the abdominal aorta by pulse wave velocity technique by analyzing ECG-based kilohertz visualization data collected at day 28 of AngII infusion using Vevo Vasc software. The in vitro aortic stiffness was determined in the abdominal aortic sections by atomic force microscopy. To evaluate the stiffness, a 2 × 2 mm segment of the abdominal aorta was obtained from mice. The aortae were opened longitudinally and the adventitial surface of each explant was fastened to a glass cover slip using cell tak.[17,33] The aortic stiffness within intact aortic explants was measured using a nano-indentation protocol with atomic force microscopy as described previously.[17,33]

Protein and PCR Array Analysis

For the analysis using a protein array, the aortic tissues extracted from experimental mice at day 28 of saline or AngII infusion (n=5 mice pooled) were snap frozen in radioimmunoprecipitation assay buffer supplemented with protease and phosphatase inhibitors. The samples were shipped in dry ice to RayBiotech for protein profiling using Quantibody Mouse Cytokine Array 4000. For PCR array, the aortic tissues from the experimental mice at day 7 of saline or AngII infusion were lysed with RNA lysis buffer. The RNA was extracted using RNeasy fibrous tissue kit (74704), and the cDNA were synthesized using iScript gDNA clear cDNA synthesis kit (BioRad, 1725035). PCR was performed on the samples using PCR array for Th1 and Th2 responses (330231, Qiagen).

Histology, Immunohistochemistry, and Double Immunofluorescence

The abdominal aortae from the experimental mice were fixed in 10% formalin and serial sections (5 μM) were obtained by cutting into 2 equal halves. The abdominal aortic sections at regular intervals (200 μM) were subjected to hematoxylin and eosin, Verhoeff-Van Gieson, and Masson trichrome stain for histoarchitectural evaluation of aneurysm. The sections obtained from these mice were further subjected to immunohistochemistry. For immunohistochemistry, the abdominal aortae were stained with antibodies for F4/80, interferon-gamma (IFNγ), Cd3, IL17, MMP2, CCN2, TGFβ1, TGFβ2, smoothelin B, and active caspase-3. The specificity of all the antibodies was confirmed using appropriate immunoglobulin G controls in place of the primary antibodies at same concentrations as described.[17] The intensity of the immunostaining was evaluated by obtaining 4 to 5 images from areas of interest (media or adventitia) at 40× from each tissue (n=5) and quantified using Fiji version of ImageJ following the software directions.[17,33] Aortic tissue sections from AngII-infused mice at day 28 were analyzed for Cd3 and F4/80 or CCAAT Enhancer Binding Protein Beta (Cebpβ) immunoreactivity using double immunofluorescence. Images were captured using LionHeart fx microscope (Biotek).[33]

Human AAA Tissue Samples and Laser Capture Microdissection

Full-thickness aortic wall tissue specimens were collected from the infrarenal abdominal aorta from patients undergoing AAA repair operations (n=6; White men, aged 60–75 years) at the Harper University Hospital in Detroit, Michigan.[4,37] Non-aneurysmal infrarenal aortic samples (n=6; White men, aged 58–78 years) were collected at autopsies and used as non-AAA controls. Samples were incubated in phosphate-buffered formalin and embedded in paraffin for histological analyses. The collection of the human tissues was obtained after informed consent and approved by the Institutional Review Board of Wayne State University in Detroit, Michigan. Medial and adventitial cells from frozen aortic sections were isolated on 10-μm cryosections with a laser capture microdissection (Arcturus PixCell II; Arcturus Engineering, Inc., Mountain View, CA) using transfer film (CapSure TF-100; Arcturus Engineering). Total RNA was extracted using Arcturus PicoPure RNA Isolation Kit (ThermoFisher, RA7007) and real-time quantitative reverse transcriptase PCR (qRT-PCR) was performed on medial and adventitial cells cDNA as described previously.[33] The primer sequences for genes are detailed in Table S1.

Real-Time qRT-PCR and Western Blotting

Total RNA was extracted from the mouse aortae using the Fibrous RNeasy kit (Qiagen) following the

manufacturer's instructions. Real time qRT-PCR was performed on CFX connect real-time PCR detection system (Bio-Rad) in triplicate. The CT value for housekeeping gene *Rpl13a* was used to standardize the gene expression. The primer sequences for genes are detailed in Table S2. For Western blotting (WB), the mouse aortic tissues were homogenized in radioimmunoprecipitation assay buffer (Thermo Scientific) supplemented with protease and phosphatase inhibitor (Sigma). The lysates were sonicated with sonic dismembrator ultrasonic processor (Fisher Scientific), centrifuged (16 000*g* for 20 minutes) at 4°C and supernatants were collected. In some experiments, RAW cells or cultured human aortic smooth muscle cells (HaSMCs; cat#CC-2572, P5-7 Lonza) were treated with IL12p40 siRNA or recombinant human IL12p40 protein (309-IL-010) with and without tumor necrosis factor-α (10 ng/mL) treatments. The cell lysates were then prepared for WB in radioimmunoprecipitation assay buffer. WB was performed in the supernatants or cell lysates with antibodies specific for CCN2, TGFβ2, TGFβ1, β-actin, MMP2, GAPDH, and corresponding horseradish peroxidase-conjugated secondary antibody (Jackson Immunoresearch, 1:10 000). Because of dissimilar expression of β-actin in the aortae of *apoE*$^{-/-}$ and DKO mice, we used non-specific band from Coomassie blue staining for normalizing the protein contents. Densitometric analysis was performed with ImageJ software.[17]

Cell isolation, Culture, and Coculture assay

Purified T cells were isolated from the spleen of apoE$^{-/-}$ or DKO mice using Dynabeads untouched mouse T cells kit (ThermoFisher). Isolated T cells were cultivated in complete Iscove's Modified Dulbecco's Media medium and activated in the presence of 1 μg/mL plate-bound anti-CD3ε (2C11) and soluble anti-CD28 (37.51) antibodies for 3 days. In some experiment, the cells were treated with AngII (200 nmol/L) for 24 hours. Bone marrow derived macrophages were prepared from *apoE*$^{-/-}$ or DKO mice as described previously.[4] The cells were then processed to extract the RNA for mRNA analysis by qRT-PCR. For co-culture assay, vSMCs derived from *apoE*$^{-/-}$ mice were co-cultured with supernatants of bone marrow derived macrophages derived from either *apoE*$^{-/-}$ or DKO mice for 48 hours. After 48 hours, the supernatants were aspirated, vSMCs were washed with cold PBS and lysed with radioimmunoprecipitation assay buffer. The protein samples were analyzed for CCN2 and MMP2 expression by WB. In some experiments, cultured HaSMCs were treated with AngII (1 μM) or human recombinant CCN2 (10 ng/mL) for 48 hours. The cells were then processed for qRT-PCR or WB and the cultured media harvested from cells were examined by gelatin zymography.

Gelatin Zymography

Cultured media were concentrated 50-fold using Amicon Ultracel- 10K centrifugal filter (Millipore, UFC801096). Concentrated media samples were mixed with zymogram sample buffer (BioRad, 161-0764). The proteins were separated in 7.5% polyacrylamide gels containing SDS and 1 mg/mL gelatin (BioRad, 170-6537). After electrophoresis gels were washed (2 × 30 minutes) with zymogram renaturation buffer (BioRad, 161-0765) while on gentle rotation. Gels were further kept in zymogram development buffer (BioRad, 161-0766) for 30 minutes at room temperature with gentle shaking. Thereafter, gels were kept in development buffer at 37°C with gentle shaking overnight. Next day, gels were stained with Coomassie blue stain, destained until bands started to appear and images were captured using gel documentation system (ChemiDoc XRS+, BioRad).

Statistical Analysis

Statistical analyses were performed using GraphPad Prism version 7.0 (GraphPad Software, Inc., CA). All continuous variables were assessed for normality and equal variance using GraphPad Prism. Continuous data were examined by Shapiro-Wilk test for normality. Two-group comparisons were performed using an unpaired 2-tailed Student *t*-test for normally distributed continuous variables. Multiple groups were compared using ANOVA followed by Tukey multiple comparison analysis or 2-way ANOVA followed by Bonferroni post-hoc tests. For data without normal distribution, non-parametric Mann-Whitney *U* test, or Kruskal–Wallis test were applied. For incidence of AAA, Fisher Exact test was performed. All data are presented as mean±SEM. $P<0.05$ was considered statistically significant.

RESULTS

IL12p40 Deficiency Does Not Prevent the Development of AAA in AngII-Induced *apoE*$^{-/-}$ Mouse Model

We previously demonstrated that *IL12p40* deficiency in the C57BL/6 mice exacerbates AAA through development of perivascular fibrosis and elastin fragmentation mediated by anti-inflammatory (M2-like) macrophages. Since wild-type mice are less susceptible to develop aneurysm, we examined the direct role of *IL12p40* deficiency in AAA pathogenesis in a standard mouse model of AAA by generating DKO mice with both *IL12p40* and *apoE* deficiency. In *apoE*$^{-/-}$ mice, the development of AAA is known to be critically driven by proinflammatory

macrophages and have a skew towards increased expression of M1-polarization markers even at naive state. Thus, in the DKO mice, we aimed to determine whether IL12p40 deficiency is sufficient to attenuate the development of AAA by antagonizing proinflammatory response. *apoE*$^{-/-}$ and DKO mice were infused with AngII subcutaneously for 28 days for induction of AAA. Surprisingly, transabdominal ultrasound imaging

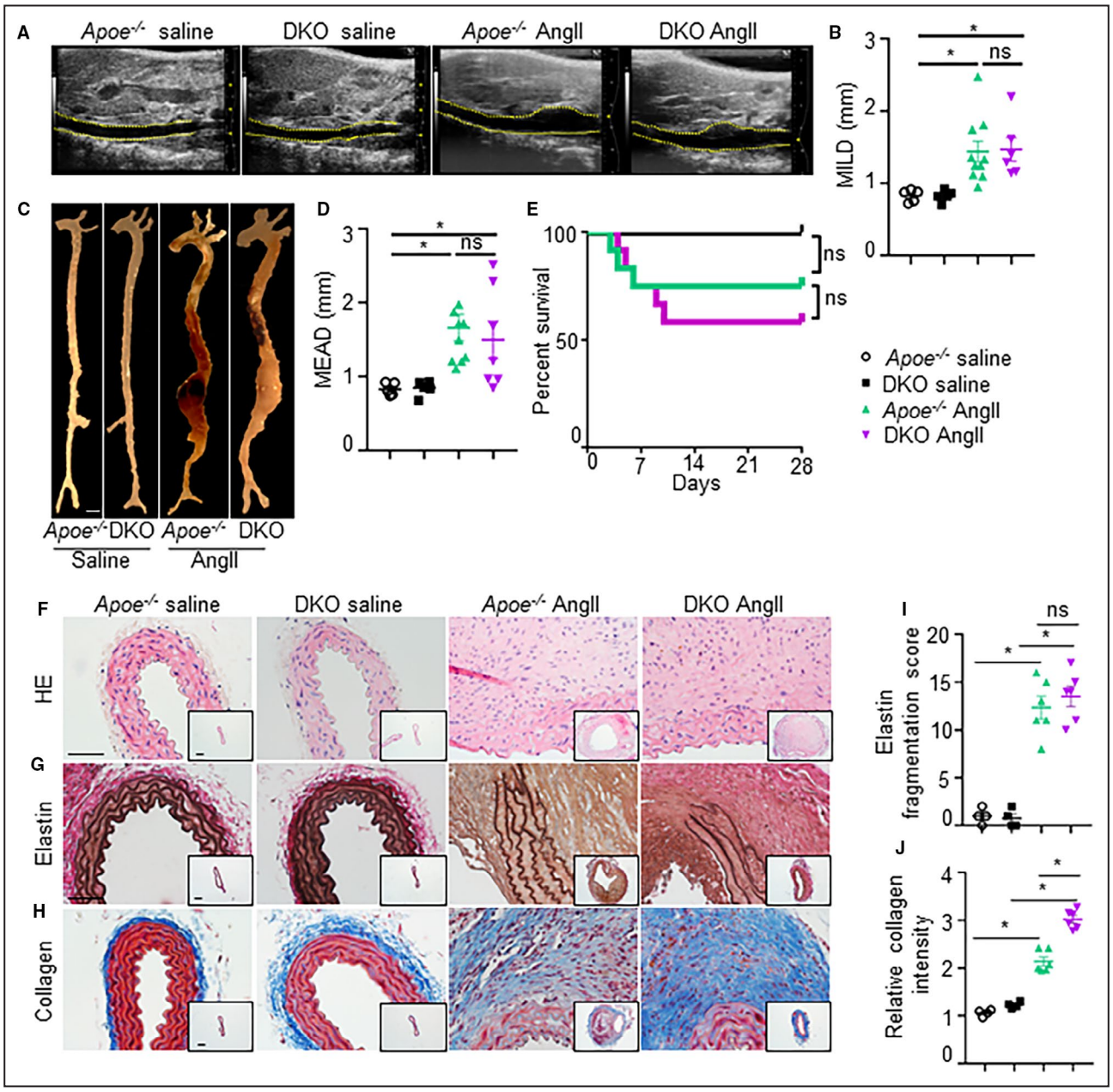

Figure 1. Similar increase in the development of abdominal aortic aneurysm in *apolipoprotein E*$^{-/-}$ and *Interleukin 12p40*$^{-/-}$; *apolipoprotein E*$^{-/-}$ (double knockout) mice in response to angiotensin II).

(**A**), Representative transabdominal ultrasound images at day 28 showing increase in the luminal expansion in *apolipoprotein E*$^{-/-}$ and double knockout mice in response to in response to angiotensin II (n=12) compared with saline infusion (n=6). Dashed yellow lines outline the lumen. (**B**), Quantification of maximal intraluminal diameters (MILD) of abdominal aorta. (**C**), Representative aortae from the experimental mice showing maximal aortic width in the suprarenal region. Scale bar=1 mm. (**D**), Quantification of ex vivo maximal external aortic diameters (MEAD) of abdominal aortae (n=6, saline; and n=12, angiotensin II). (**E**), Graph showing survival curve in *apolipoprotein E*$^{-/-}$ and double kncokout mice in response to saline or angiotensin II. (**F**–**H**), Transverse sections of aortae stained with hematoxylin and eosin, Verhoeff-Van Gieson, and trichrome staining staining illustrating the extent of abdominal aortic aneurysm progression, elastin fragmentation, and collagen for fibrosis, respectively, at day 28 in the experimental mice (n=6). The insets represent the 4× images of corresponding 40× pictures. (**I** and **J**), Quantification of medial elastin degradation and collagen deposition in experimental groups (n=6 for each group). Kruskal–Wallis test was applied for statistics in **B** and **D**. Log-rank test was used for survival curve in **E**. Tukey multiple comparisons test was used in **I** and **J**. Scale bar=50 μm in **F**–**H**. **P*<0.05, ns=non-significant.

showed similar increase in the luminal expansion of the suprarenal aorta of both the groups at day 28 of AngII (1.44±0.14 in *apoE*$^{-/-}$ AngII versus 1.46±0.16 in DKO) (Figure 1A and 1B). Macroscopically, the increase in maximal aortic diameter of suprarenal aorta in response to AngII in both *apoE*$^{-/-}$ and DKO mice was similar (1.66±0.18 in *apoE*$^{-/-}$ AngII versus 1.49±0.25 in DKO) (Figure 1C and 1D). Interestingly, a modest increase in aortic dissection-mediated mortality in DKO mice was observed compared with *apoE*$^{-/-}$ mice in response to AngII (5 out of 12 versus 3 out of 12; Figure 1E and Figure S1A). The increase in the dilations of the thoracic aorta was also similar between *apoE*$^{-/-}$ and DKO mice at day 28 of AngII (Figure S1C–F). No significant changes in distensibility and radial strain were observed in the *apoE*$^{-/-}$ or DKO mice in response to AngII (Figure S2).

Hematoxylin and eosin and elastin staining of aorta in *apoE*$^{-/-}$ and DKO mice did not show any observable difference in the histoarchitectural features in the aneurysmal tissues (Figure 1F and 1G). Elastin staining of aorta from both *apoE*$^{-/-}$ and DKO mice infused with AngII displayed similar fragmentation of the elastin layer (Figure 1G and 1I). However, the extent of collagen deposition examined by Masson trichrome staining was significantly higher in the aortae of DKO than *apoE*$^{-/-}$ mice infused with AngII indicating that *IL12p40* deficiency promotes aortic fibrosis (Figure 1H and 1J). Interestingly, similar increase in active caspase-3 immunoreactivity was observed in the medial layer of the aorta suggesting that fibrotic effects of *IL12p40* deficiency in aneurysmal mice have no significant effect on the apoptotic cell death of vSMCs (Figure S3). Overall, histological examination of aneurysmal tissues provides only limited information whether pathogenesis of AAA is different in these experimental groups.

DKO Mice Demonstrate Decreased Proinflammatory Macrophages Infiltration But Increased Synthetic-vSMC Phenotype and T Cells in the Aortic Lesions

To determine mechanistically how predominance of anti-inflammatory macrophages with IL12p40 deficiency can lead to the development of AAA, we performed a protein array. Abdominal aortae were extracted from the experimental mice (pooled from n=5 in each group) and subjected to protein profiling using quantibody Mouse Array (RayBiotech) to examine the quantitative changes in the cytokines which are differentially expressed in the AAA lesions of *apoE*$^{-/-}$ and DKO mice at baseline and in response to AngII (Table 1). The full name of protein abbreviations are detailed in Table S3. The analysis of a total of 200 proteins showed 3 prominent pathways dysregulated in these 2 distinct strains of aneurysmal mouse models: inflammatory cytokines, synthetic vSMC phenotype, and Th17-related cytokines. Expectedly, the expression of proinflammatory cytokines including IL1ra, MCP1 (monocyte chemoattractant protein), macrophage colony-stimulating factor (m-CSF), MIP-2 (macrophage inflammatory protein 2), tumor necrosis factor-α, Igfbp3, p-selectin, and CRP (C-reactive protein) were increased in the *apoE*$^{-/-}$ mice in response to AngII than baseline (Table 1). The expression of these proinflammatory cytokines was reduced to <60% in the DKO mice as compared with *apoE*$^{-/-}$ with AngII (Table 1).

The expression of cytokines related to synthetic vSMCs including activin receptor-like kinase-1 (ALK-1), artemin, betacellulin, and clusterin were higher in the aortic tissue of DKO mice than *apoE*$^{-/-}$ mice at baseline (Table 1). In response to AngII, the expression of cardiotrophin-1, artemin, and betacellulin increased moderately in the *apoE*$^{-/-}$ mice, whereas, the expression of these cytokines along with clusterin and milk fat globule-EGF factor 8 were increased markedly in the aortic tissue of DKO compared with *apoE*$^{-/-}$ mice (Table 1). The expression of ALK-1, a disintegrin and metalloproteinase with thrombospondin motifs, and vascular endothelial growth factor B remained higher in the DKO mice in response to AngII and were minimal in the *apoE*$^{-/-}$ mice.

The T-cell related cytokines including 4-1BB, IL22, Cd27, transmembrane activator and CAML interactor, IL7ra, and Cd40l were higher in the DKO than *apoE*$^{-/-}$ mice at baseline (Table 1). In response to AngII, the expression of Cd27, transmembrane activator and CAML interactor, IL7ra, and Cd40Ll increased moderately in the *apoE*$^{-/-}$ mice, whereas, the expression of these cytokines along with 4-1BB, Interleukin-17E (IL17e), increased markedly in the DKO aortae. The expression of 4-1BB, IL22, and IL17e remained negligible in the *apoE*$^{-/-}$ mice at baseline or in response to AngII. Our study also revealed novel cytokines including Shh-N, testican-3, marapsin, and Nov/CCN3 increased in the aortic tissues of DKO mice as compared with *apoE*$^{-/-}$ at baseline or in response to AngII (Table 1).

T cells are a dominant population in human AAAs and their infiltration occurs at an early stage of the disease in experimental mice.[38,39] Because of novel findings in the T-cell associated cytokines in DKO mice, we extracted cDNA from the AAA lesions at day 7 from both these groups and subjected to RT^2 Profiler PCR Array Mouse Th1 and Th2 cytokines (PAMM-034Z, Qiagen; Table 2). Consistent with the RayBiotech cytokine array data, we observed increased mRNA expression of T-cell related cytokines, mainly Th2 and Th17 including *IL10, Cd4, IL4ra, IL7r*, and *Cebpβ* in the aortic tissues of DKO mice compared with *apoE*$^{-/-}$ in response to AngII (Table 2). We confirmed the decreased expression

Table 1. Protein Array Data Showing Differential Expression of Cytokines in the Aortic Tissue of Experimental Mice as Determined Using Quantibody Mouse Cytokine Array 4000 (RayBiotech)

Protein Name	Gene Name	Uniport ID	*apoE*$^{-/-}$ saline (pg/mL)	DKO saline (pg/mL)	Ratio 1	*apoE*$^{-/-}$ AngII (pg/mL)	DKO AngII (pg/mL)	Ratio 2
T helper 17-related cytokines								
Ang-3	*Agpt3*	Q9WVH6	nd	nd	nd	nd	2293.8	2293.8
4-1BB	*Tnfrsf9*	P20334	nd	174.9	174.9	nd	1251.1	1251.1
IL-22	*Iltif*	Q9JJY9	nd	378.4	378.4	nd	266.4	266.44
IL-17F	*Il17F*	Q7TNI7	nd	nd	nd	nd	93.9	93.9
Prolactin	*Prl*	P06879	nd	nd	nd	nd	85.4	85.4
IL-20	*Zcyto10*	Q9JKV9	nd	nd	nd	nd	76.9	76.9
IL-17E	*Il25*	Q8VHH8	nd	nd	nd	4.9	245.5	50.65
IL-2Ra	*Il2ra*	P01590	nd	nd	nd	nd	7.9	7.94
CD-27	*Tnfrsf7*	P41272	39.5	264	6.7	409.2	2784.8	6.81
Taci	*Tnfrsf13B*	Q9ET35	51.1	214.3	4.2	215.7	982.8	4.56
IL-7Ra	*Il7r*	P16872	nd	930	930	815.8	2542.3	3.12
IL-13	*Il13*	P20109	nd	nd	nd	nd	16.9	16.9
Cd-40L	*Tnfsf5*	P27548	49.4	426.1	8.6	554.2	1118.8	2.02
Synthetic vascular smooth muscle cell-related cytokines								
Alk-1	*Slpi/Wap4*	Q61288	nd	137.8	137.8	nd	574	574.04
Adamts-1	*Adamts1*	P97857	nd	nd	nd	nd	262.8	262.81
Ct-1	*Ct1*	Q60753	nd	239.5	239.5	14.4	953.2	66.2
Artemin	*Artn/Evn*	Q9Z0L2	nd	49.6	49.6	74.9	867.7	11.58
VEGF-B	*Vegfß/Vrf*	P49766	nd	nd	nd	nd	8.4	8.36
Betacellulin	*Btc*	Q05928	11.4	17.9	1.6	26.8	109.3	4.08
Clusterin	*Clu/apoJ*	Q06890	25497.2	37284.8	1.5	19867.9	53608.3	2.7
Mfg-e8	*Mfge8*	P21956	7985	9301	1.2	7232.1	17214.3	2.38
VEGF R1	*Emrk2*	P35969	386.6	551.2	1.4	701.1	1409.9	2.01
Novel cytokines								
Shh-N	*Shh/Hhg1*	Q62226	nd	nd	nd	nd	190.9	190.94
Testican 3	*Spock3*	Q8BKV0	880.8	1648.7	1.9	1472.9	5938.8	4.03
Marapsin	*Prss27/Mpn*	Q8BJR6	5430	7455.8	1.4	8772.8	20531.6	2.34
Prostasin	*Prss8/Cap1*	Q9ESD1	1361.3	4709.7	3.5	2234.3	4901.5	2.19
MMP-10	*MMP10*	O55123	1019.4	1159.5	1.1	1013.3	2194.4	2.17
Nov/CCN3	*Igfbp9*	Q64299	2609.4	2432.7	0.9	8172.5	17169.3	2.1
Macrophage-related cytokines								
IL-1ra	Il1rn	P25085	nd	nd	nd	2553.1	18.9	0.01
Mcp-1	Ccl2	P10148	nd	nd	nd	33.3	nd	0.03
Kc	Cxcl1	P12850	nd	nd	nd	16.3	nd	0.06
m-Csf	Csf1	P07141	nd	nd	nd	23.2	5.4	0.23
Mip-2	Cxcl2	P10889	nd	nd	nd	3.9	1.0	0.25
Tnf-α	Tnf	P06804	nd	nd	nd	3.9	nd	0.25
Igfbp-3	Ibp3	P47878	290.0	193.2	nd	1973.5	666.9	0.34
Sdf-1α	Cxcl12	P40224	nd	nd	nd	307.5	132.6	0.43
Lix	Cxcl5	P50228	nd	nd	nd	64.3	28.2	0.44
IL-6	IL6	P08505	nd	nd	nd	51.1	24.0	0.47
CRP	Crp/Ptx1	P14847	nd	nd	nd	15 212.2	8248.3	0.54
Gm-Csf	Csf2	P26955	nd	nd	nd	168.7	94.6	0.56
p-Selectin	Selp	Q01102	1064.2	2275.6	2.14	5734.7	3338.0	0.58

Ratio 1=DKO saline/*apoE*$^{-/-}$ saline. Ratio 2=double knockout angiotensin II/*apolipoprotein E*$^{-/-}$ angiotensin II. We used value of nd=1 to calculate ratio for some proteins in which the expression was not detected. nd indicates not detected.

Table 2. Genes Upregulated by *Interleukin 12* Deficiency at Day 7 of AngII-Infusion in Aorta

Symbol	GenBank	UniGene	Full Name	Fold increase in DKO mice compared with apoE$^{-/-}$ mice
IL5	NM_010558	Mm.4461	Interleukin 5	7.42
Gfi1	NM_010278	Mm.2078	Growth factor independent 1	3.97
Ccr4	NM_009916	Mm.1337	Chemokine (C-C motif) receptor 4	3.75
Cebpß	NM_009883	Mm.439656	CCAAT/enhancer binding protein (C/EBP), beta	3.71
Junb	NM_008416	Mm.1167	Jun-B oncogene	3.31
Tnf	NM_013693	Mm.1293	Tumor necrosis factor	3.09
IL18r1	NM_008365	Mm.253664	Interleukin 18 receptor 1	2.99
Spp1	NM_009263	Mm.288474	Secreted phosphoprotein 1	2.78
Tnfrsf8	NM_009401	Mm.12810	Tumor necrosis factor receptor superfamily, member 8	2.7
IL2	NM_008366	Mm.14190	Interleukin 2	2.65
Cd4	NM_013488	Mm.2209	CD4 antigen	2.45
Socs3	NM_007707	Mm.3468	Suppressor of cytokine signaling 3	2.43
Socs5	NM_019654	Mm.126885	Suppressor of cytokine signaling 5	2.32
IL4ra	NM_001008700	Mm.233802	Interleukin 4 receptor, alpha	2.17
IL7r	NM_008372	Mm.389	Interleukin 7 receptor	2.02
Cd28	NM_007642	Mm.255003	CD28 antigen	2.01

of *IL12p40* and increased expression of *IL10*, *Rorγt, Foxp3,* and *Cebpβ* in the aortic tissues of DKO mice at day 7 of AngII infusion (Figure 2A). The increase in the expression of *IL17a, TGFβ2, Rorγt,* and *Cebpβ* was also confirmed in T cells isolated from the spleen of DKO mice by qRT-PCR (Figure S4A). Interestingly, the expression of Cebpβ was downregulated modestly in the bone marrow derived macrophages of DKO mice as compared with *apoE*$^{-/-}$ at the baseline (Figure S4B). Expectedly, the expression of proinflammatory cytokines including *IL12p40, IFNγ,* and *IL6* were significantly decreased, and the expression of anti-inflammatory cytokine *Cd206* was significantly increased (Figure S4B).

The immunohistochemical staining of aortic tissues from *apoE*$^{-/-}$ mice displayed F4/80^{+} and IFNγ^{+} macrophages in the adventitial layer, which was minimal in the aortic tissues from DKO mice (Figure 2B through 2E, $P<0.01$). Surprisingly, Cd3^{+} and IL17^{+} immunostaining, which are predominantly recognized as proinflammatory Th17 cells, was increased near the regions of elastin breaks in the aneurysmal tissues of DKO mice, and was minimal in *apoE*$^{-/-}$ mice (Figure 2F through 2I, $P<0.01$). Because of differential expression of Cebpβ in the aorta, T cells and macrophages, and its association with Th17 cells,[40] we performed double immunofluorescence to further study these interesting observations. Indeed, we observed colocalization of Cd3^{+} cells with Cebpβ^{+} cells in the aortic tissues from AngII-infused DKO mice, which was predominant in the regions of visible elastin breaks. Whereas, in the *apoE*$^{-/-}$ mice, only a weak colocalization between Cd3^{+} and Cebpβ^{+} cells was observed. However, no such colocalization of Cebpβ^{+} cells with F4/80 + macrophages was observed in both these experimental groups (Figure S4D). These data indicate that the AAA develops differently in these 2 strains of mice with unique mechanism. The proinflammatory response is predominant in the *apoE*$^{-/-}$ mice; whereas the DKO mice exhibit anti-inflammatory/fibrotic response.

Increased CCN2-Dependent MMP2 expression in the Aorta and vSMCs of DKO Mice

The association of IL12 deficiency with synthetic vSMC phenotype in the cytokine array seemed very intriguing. CCN2 (previously known as connective tissue growth factor; CTGF), a downstream target of TGFβ signaling, is a potent modulator of synthetic vSMC phenotype. We have previously shown that CCN2 expression is increased in the abdominal aorta of human AAA, however, its cell-specificity and association with IL12 deficiency has not been determined.[33,41] The mRNA expression of CCN2 signaling pathway including Smad2, TGFβ2 and CCN2 was significantly increased in the aorta of DKO mice compared with *apoE*$^{-/-}$ mice in response to AngII (Figure S5). WB of the protein extract from the abdominal aortae demonstrated increased CCN2 expression in the aorta of DKO mice as compared with *apoE*$^{-/-}$ in the saline-treated mice (Figure 3A). In

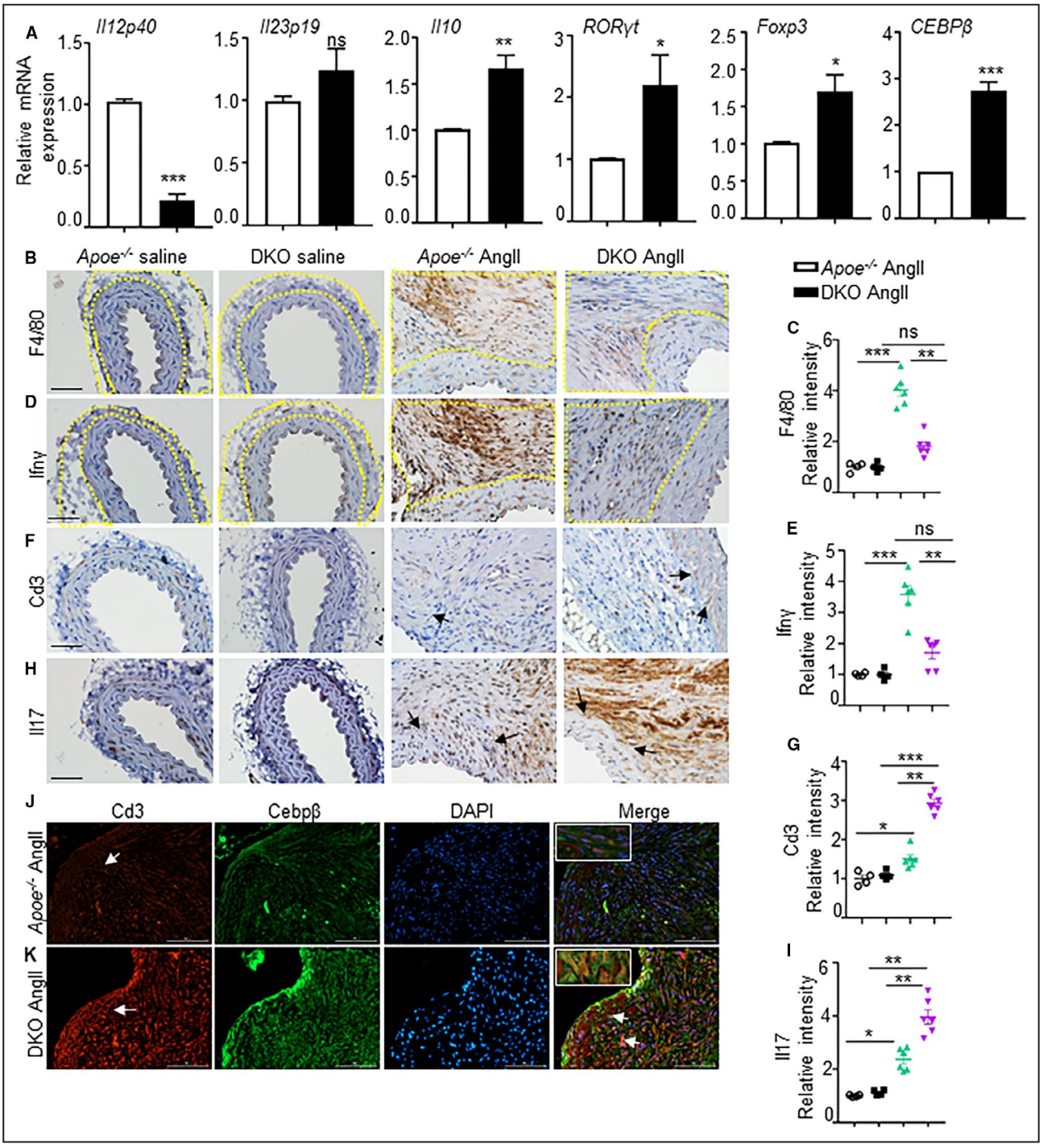

Figure 2. Double knockout mice exhibit increased T-cell infiltration in the aortic lesions.
(**A**), mRNA expression of various cytokines in the aortic tissues of *apolipoprotein E*$^{-/-}$ and double knockout mice at day 7 of angiotensin II infusion. (**B**-**E**) and (**F**-**I**), Immunohistochemistry showing expression of F4/80 (total mature macrophages), interferon-γ (M1 macrophage marker), Cd3 (T cells), and interleukin-17 expression and their quantifications in the adventitial region of aortic tissue at day 28 in experimental mice. Yellow dotted lines in **B** and D outline the adventitial region. (**J** and **K**), Cd3 and Cebpβ expression and their co-localization in the aortic tissues from angiotensin II-infused *apolipoprotein E*$^{-/-}$ and double knockout mice. *P<0.05, **P<0.01; ***P<0.001, ns=non-significant in Tukey multiple comparisons test. Scale bar=50 μm.

response to AngII, moderate increase in the CCN2 contents was observed in the *apoE*$^{-/-}$ mice, whereas this expression was significantly increased in the DKO mice (P<0.01). Interestingly, TGFβ2 protein contents were significantly increased in the abdominal aorta of DKO mice in response to AngII, whereas

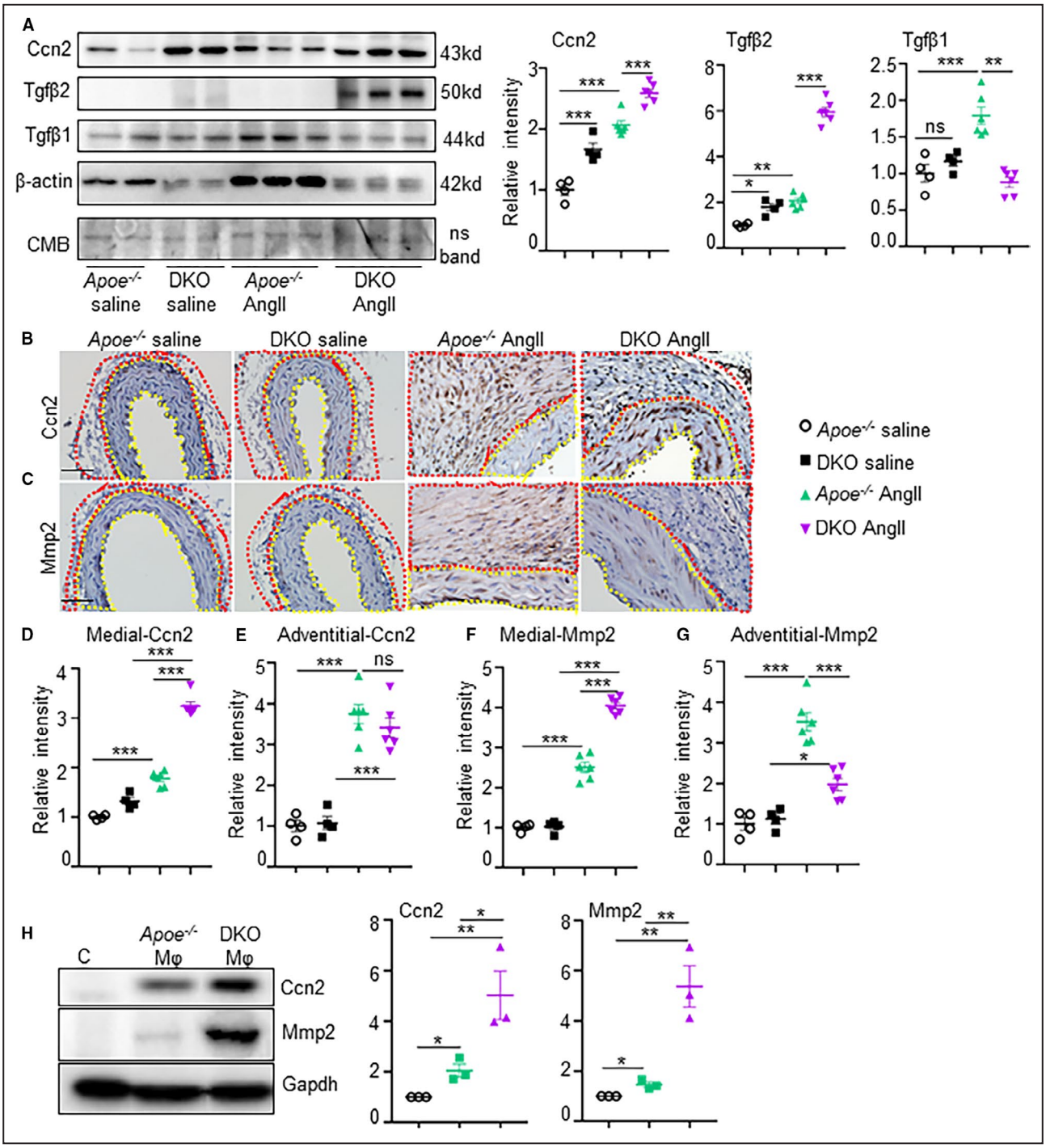

Figure 3. ***Interleukin 12p40*** **deficiency increases CCN2 (cellular communication network factor 2) expression in the vascular smooth muscle cells rich medial layer of aorta.**

(**A**), Western blots showing expression of CCN2, transforming growth factor β2, and transforming growth factor-β1 from the aortic tissues of experimental mice and its quantification (n=4 for saline and 6 for angiotensin II groups). (**B**–**G**), Immunohistochemistry showing confirmatory expression of CCN2 and matrix metalloproteinase 2, and its quantifications in the medial and adventitial regions from the aortic tissues of experimental mice at day 28 (n=6). Yellow dotted lines in B and C outline the medial region, whereas red dotted lines in B and D outline the adventitial region. (**H**), Western blot of vascular smooth muscle cells and its quantification from cells treated with supernatants derived from macrophages of *apolipoprotein E*$^{-/-}$ or double knockout mice showing expression of CCN2 and matrix metalloproteinase 2 (representative of 3 independent experiments). *P<0.05, **P<0.01, ***P<0.001, ns=non-significant in Tukey multiple comparisons test (**D**–**G**) and unpaired t-test (**H**). Scale bar=50 μm. CMB=Coomassie Blue Stain.

TGFβ1 were predominantly increased in the *apoE*$^{-/-}$ mice (Figure 3A). To examine the cellular source of CCN2 in these mice, we performed immunohistochemistry. CCN2 expression was significantly increased in the adventitial layer of *apoE*$^{-/-}$ mice in response to AngII (red boundary; Figure 3B and 3E), whereas the increase in the medial layer was moderate (yellow boundary; Figure 3B and 3D). In contrast, CCN2 immunostaining was increased in the medial layer of DKO mice and was significantly higher than in *apoE*$^{-/-}$ mice (yellow boundary; Figure 3D and 3E). The expression of CCN2 in DKO mice was opposite to *apoE*$^{-/-}$, with increased staining observed in the medial layer compared with adventitia (Figure 3C through 3E). Notably, because of the enrichment of CCN2 in the medial layer of DKO mice, we speculate that the cellular source of CCN2 in DKO mice is predominantly vSMCs and it plays a role in the phenotypic changes of vSMCs from contractile to synthetic during pathogenesis of AAA.

Next, we examined whether IL12p40 deficiency-mediated increase in CCN2 plays a pathogenic role in AAA pathogenesis by increasing MMPs in the medial aortic layer. Immunostaining of MMP2 was increased predominantly in the adventitia of aorta in *apoE*$^{-/-}$ mice infused with AngII, although moderate increase was observed in the medial layer (Figure 3C, 3F, 3G). Interestingly, MMP2 immunostaining was significantly increased in the aortic tissue of DKO mice compared with *apoE*$^{-/-}$ and was predominantly localized in the medial aortic layer (Figure 3C and 3F). It is important to note that the major source of IL12p40 in the vasculature is myeloid cells, whereas vSMCs and fibroblasts have minimal expression of IL12.[17,42] To examine if the interactions between anti-inflammatory/profibrotic macrophages influence CCN2/MMP2 signaling, we set up a co-culture system in which vSMCs were cultured in the presence or absence of media derived from macrophage cultures originating from *apoE*$^{-/-}$ versus DKO mice. Significant increase in CCN2 and MMP2 expression in the vSMCs was observed when cell-culture media from DKO macrophages was added to vSMCs as compared with media from *apoE*$^{-/-}$ macrophages (Figure 3H). In addition, we examined the expression of CCN2 in the HaSMCs treated with IL12p40 siRNA or the recombinant human IL12p40 protein. Expectedly, there was no change in the CCN2 expression as the basal expression of IL12p40 is minimal in the vSMCs (Figure S6A). Similarly, we examined the TGFβ2 expression in macrophages treated with IL12p40 siRNA or recombinant human IL12p40 protein. Interestingly, TGFβ2 expression was increased in macrophages with IL12p40 siRNA and decreased with recombinant human IL12p40 treatment (Figure S6B). Taken together, these data demonstrate that the deleterious effects of *IL12p40* deficiency on aortic dysfunctions are probably mediated by macrophages induced TGFβ2 and their crosstalk with vSMCs to induce CCN2 signaling in the vSMC-rich medial layer. These data also suggest that anti-inflammatory macrophages could be the potential source of increased CCN2 expression in vSMCs and MMP2 activity mediating the matrix degradation in the DKO mice. Activation of MMPs in the *apoE*$^{-/-}$ mice in response to AngII on the other hand is mediated by proinflammatory macrophages as shown extensively by others and us previously.[4,6,43]

Differential Expression of CCN2 in the Vascular Cells of Human Aortic Tissue

Consistent with these data and our previous studies,[41] we observed an increased immunostaining of CCN2 in human AAA, which was primarily localized in the medial layer of aneurysmal tissue (Figure S7). Considering the complexity of the disease, we used laser capture microdissection to examine the differential expression of CCN2-associated genes in the media and adventitia (Figure 4A through 4F). The mRNA expression of CCN2 in the medial layer of AAA tissues was increased by ≈3-fold compared with medial layer of non-AAA (P<0.01; Figure 4G). The expression of CCN2 in the adventitia of non-AAA was ≈4-fold higher than medial layer of non-AAA and did not change in AAA tissues. This is consistent with the literature that constitutive expression of CCN2 in the adventitia does not interfere with the contractile functions of the medial layer.[44] Expression of *TGFβ2*, smoothelin B, and the alpha 1 chain of type I collagen followed the same trend as CCN2 in these tissues albeit at lesser extent (Figure 4H, 4J, and 4K). Expression of *TGFβ1* on the contrary was increased in the adventitia of AAA compared with adventitia of non-AAA or media of AAA (Figure 4I). We further demonstrated that treatment of HaSMCs with human recombinant CCN2 (10 ng/mL) for 24 hours increased mRNA expression of osteopontin (*OPN*; P <0.001) and *MMP2* (P <0.01) but not *MMP9* (Figure 4L). We also demonstrated that treatment of HaSMCs with human recombinant CCN2 and AngII (1 μM) for 24 hours increased the protein expression and proteolytic activity of MMP2 in HaSMCs as shown by WB and gelatin zymography, respectively (Figure 4M). This increased expression of CCN2 and MMP2 was not observed in fibroblasts treated with AngII or human recombinant CCN2 (data not shown).

Ccn2 Haploinsufficiency Attenuates Elastase-Induced Aortic Dilations

To confirm the direct role of CCN2 on aortic remodeling and fibrosis, we infused AngII in *Ccn2*$^{+/+}$ and

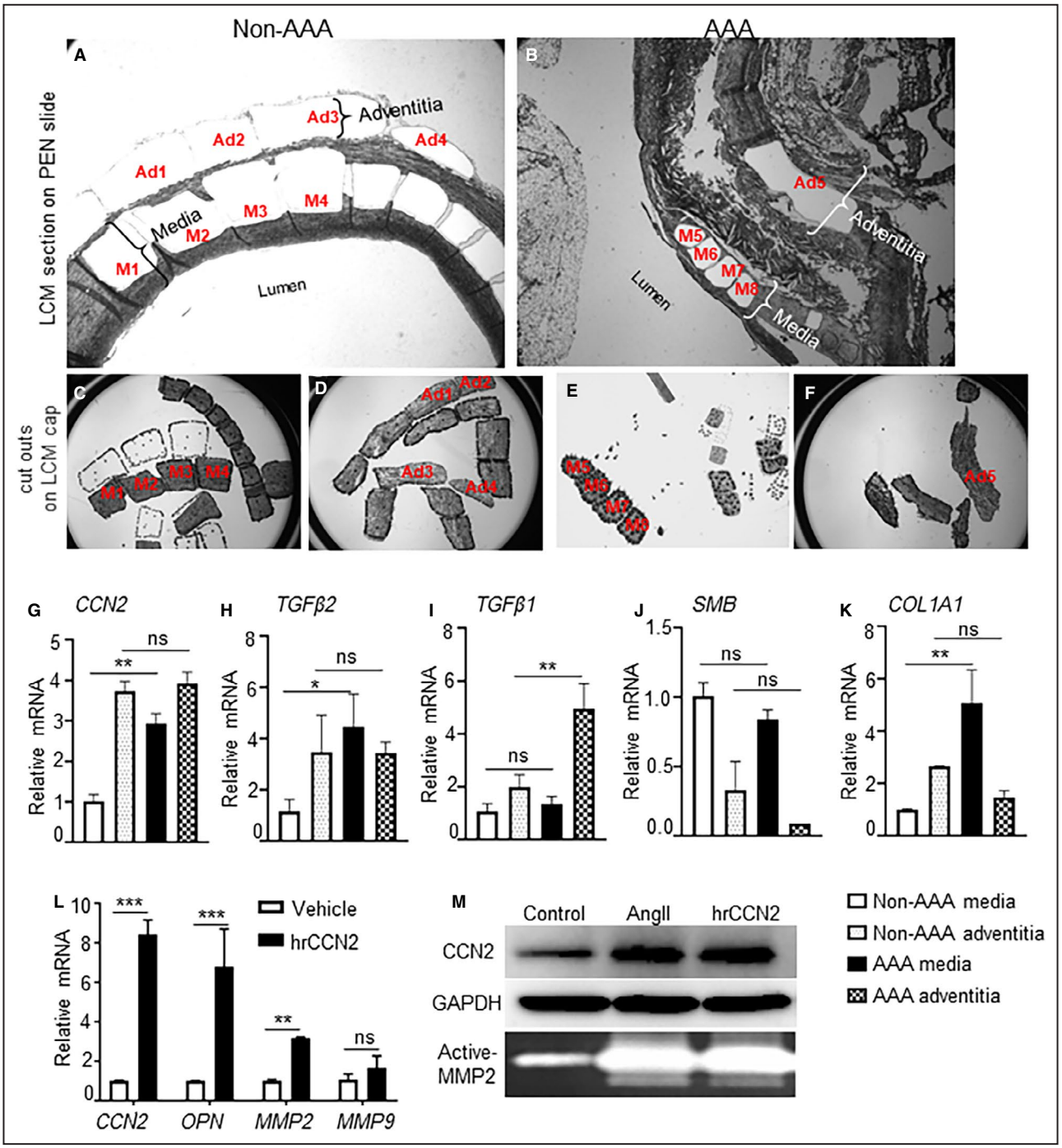

Figure 4. Increased CCN2 (cellular communication network factor 2) expression in the media layer of human abdominal aortic aneurysm.

(**A**–**F**), Images obtained during laser capture microdissection to separate the medial and adventitial regions of human non-abdominal aortic aneurysm (AAA) and AAA tissue sections (n=4 for both AAA and non-AAA isolated at the Core facility of The University of Missouri. Representative example of human aortae for gene expression. M1-M4: medial layer cells from non-AAA; Ad1-Ad4: adventitial layer cells from non-AAA in **A**, **C,** and **D**. M5-M8: medial layer cells from AAA; Ad5: adventitial layer cells from AAA in **B**, **E,** and **F.** The 2 layers were recognized by the presence or absence of elastin fragments in the serial sections stained with von-Gieson. (**G**–**K**), (**L**), mRNA expression of various genes in the human aortic smooth muscle cells treated with human recombinant CCN2 (10 ng/mL) for 48 hours. (**M**), Representative Western blot to show CCN2 expression and gelatin zymography showing active-matrix metalloproteinase 2 in the human aortic smooth muscle cells (Lonza; CC-2571) treated with AngII (1 μM) or human recombinant CCN2 (10 ng/mL) for 24 hours (average from 3 independent experiments). *P<0.05, **P<0.01, ***P<0.001, ns=non-significant in Tukey multiple comparisons test. AngII indicates angiotensin II; and PEN, polyethylene naphthalate membrane.

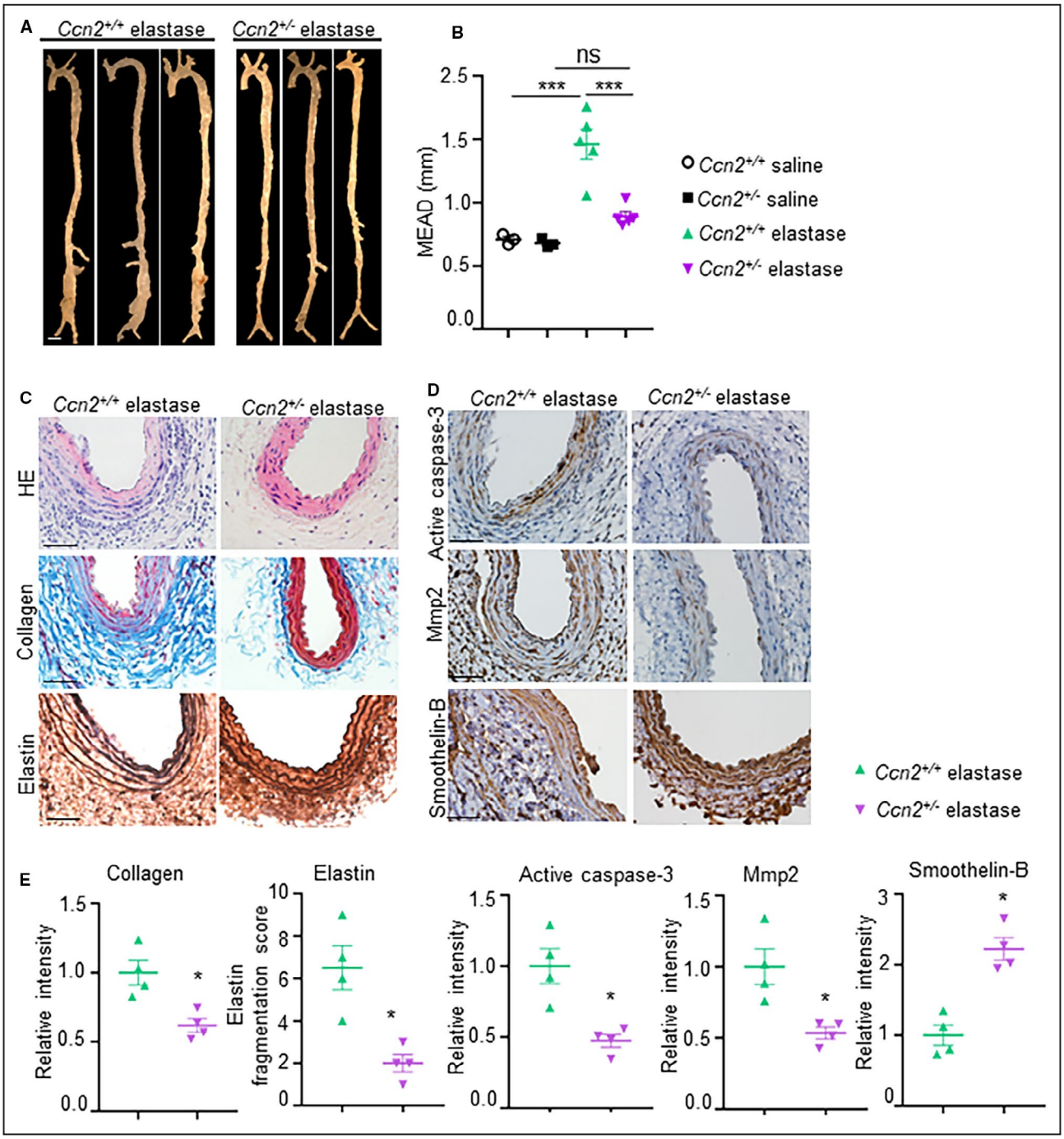

Figure 5. CCN2 (cellular communication network factor 2) deficiency reduces the development of abdominal aortic aneurysm in elastase-induced mouse model of abdominal aortic aneurysm.

(**A**), Representative aortae from the elastase-induced experimental mice at day 14 showing maximal aortic width in the infra-renal region. Scale bar, 1 mm. (**B**), Quantification of external diameter of infrarenal aortae (n=3 for controls, n=5 for *Ccn2*$^{+/+}$ elastase and *Ccn2*$^{+/-}$ elastase). (**C**), Representative images of infrarenal aorta stained with hematoxylin and eosin, trichrome, and Verhoeff-Van Gieson staining illustrating the extent of abdominal aortic aneurysm progression, fibrosis and elastin fragmentation, respectively, at day 14 in the experimental mice. (**D**), Representative immunohistochemistry images showing expression of active caspase-3, matrix metalloproteinase 2, and smoothelin-B in the aortic tissues at day 14 in experimental mice (n=5). (**E**), Quantification of collagen, elastin, active caspase-3, matrix metalloproteinase 2, and smoothelin B in the aortic tissues of experimental mice (n=4). Scale bar=50 μm. ***P<0.001, ns=non-significant in Tukey multiple comparisons test.

Ccn2$^{+/-}$ mice. At day 7 of AngII, transabdominal ultrasound imaging showed a significant decrease in pulse wave velocity (marker of aortic stiffness) in the *Ccn2*$^{+/-}$ mice as compared with *Ccn2*$^{+/+}$ (Figure S8A). Atomic force microscopy-assessed aortic stiffness remained significantly lower in the *Ccn2*$^{+/-}$ mice as

compared with *Ccn2*$^{+/+}$ at day 7 of AngII (Figure S8B). These data indicate that the *Ccn2* deficiency has protective effects on aortic stiffening during early stages of the disease. We also observed a decrease in the expression of TGFβ2, IL17, MMP2, tumor necrosis factor-α, and IL6 in the aortic tissue of *Ccn2*$^{+/-}$ mice at day 7 of AngII as compared with *Ccn2*$^{+/+}$ with same regimen (Figure S8C-I). Proteolytic activity of the aortic tissue was also reduced in the *Ccn2*$^{+/-}$ mice compared with *Ccn2*$^{+/+}$ at day 7 of AngII (Figure S8J). Finally, we performed aneurysmal studies on the *Ccn2*$^{+/-}$ mice to determine the changes in the aorta in response to elastase. The experimental mice were infused with elastase directly in the infrarenal aorta using aseptic sterile technique.[35] At day 14 of elastase treatment, the macroscopic examination showed significant increase in the maximal external aortic diameter in the *Ccn2*$^{+/+}$ mice, whereas in the *Ccn2*$^{+/-}$ mice, this increase was significantly less compared with *Ccn2*$^{+/+}$ (1.46±0.12 in *Ccn2*$^{+/+}$ elastase versus 0.89±0.04 in *Ccn2*$^{+/-}$ elastase mice) (Figure 5A and 5B). Histologically, adventitial thickening, collagen deposition, and elastin fragmentation remained minimal in the *Ccn2*$^{+/-}$ mice as compared with *Ccn2*$^{+/+}$ at day 14 of elastase (Figure 5C). Decreased immunostaining of CCN2, active caspase-3, and MMP2 were observed in the medial layer of *Ccn2*$^{+/-}$ mice as determined by immunohistochemistry (Figure 5D and 5E and Figure S9). Concomitantly, smoothelin-B expression was increased by *Ccn2* deficiency in the medial layer (Figure 5D and 5E). Collectively, these findings confirmed that *Ccn2* deficiency preserves the vSMCs contractile phenotype and decreases aortic stiffness and proteolytic activity of the aorta.

DISCUSSION

Multiple studies have shown increased IL12 expression and its linear correlation with proinflammatory response in human AAA and experimental mouse models.[35,45,46] However, direct roles of IL12 deficiency in AAA have not been examined. In this regard, we report here that IL12p40 knockout mice (*IL12p40*$^{-/-}$) generated with *apoE*$^{-/-}$ deficiency (*IL12p40*$^{-/-}$*apoE*$^{-/-}$*; DKO* mice) do not prevent against AAA development in response to AngII. These mice depict increased fibrotic and proteolytic events associated with increased TGFβ2/CCN2 signaling in the aortic tissues and significantly increased expression of MMP2 in the medial layer of aorta enriched with vSMCs. Increased CCN2 also correlated with MMP2 in the medial layer of human AAA. Finally, we show that *Ccn2* haploinsufficiency reduces aortic dilations in response to elastase infusion, associated with decreased apoptotic cell death and MMP2 contents. Overall, these data suggest that IL12p40 deficiency in *apoE*$^{-/-}$ mice contribute to matrix remodeling and ECM degradation by a novel mechanism consisting of CCN2/MMP2 signaling.

Critical events during the development of AAA in humans at an early stage of the disease remain elusive. Therefore, understanding the pathogenesis of AAA predominantly relies on the mouse models, which mimic AAA on a short scale. In these mouse models, transmural infiltration of myeloid cells and progressive differentiation of the vSMCs from contractile to synthetic phenotype has been suggested as critical steps.[25,29,33,41] In this context, role of proinflammatory macrophages in the development of AAA is well established, however, the direct roles of anti-inflammatory macrophages and synthetic vSMC phenotype are not clearly known. Using an unbiased approach of protein array, we identified defects in vSMC phenotype and Th17-related cytokines in the aortic tissues of DKO mice during AAA development in addition to increased anti-inflammatory response. We also identified increased expression of a matricellular protein, CCN2, in the medial layer of aortic tissues of DKO mice and human AAA tissues, which positively correlated with MMP2. CCN2 is minimally expressed in the naïve-contractile vSMCs, and is induced in the synthetic vSMCs under diseased conditions. However, the direct roles for CCN2 in the development of AAA are unknown. Our studies indicate that AAA development in DKO mice is mediated by TGFβ2/CCN2 crosstalk in the absence of proinflammatory environment. Decreased aortic dilations and apoptotic cell death in the CCN2-deficient mice in response to elastase treatment are further suggestive of active role for CCN2 in AAA.

The pathogenesis of AAA in the AngII-induced *apoE*$^{-/-}$ mice is well characterized and involves the activation of proinflammatory cytokines including IL6, IL12, IL1β, and Mcp1. In contrast, profound changes in the ECM of the aortic wall, mediated by cellular secretion of CCN2 and MMP2, represent a critical hallmark in DKO mice. Since the constitutive and inducible expression of IL12 in the vascular cells including vSMCs and fibroblasts is minimal, it is speculative that interactions between anti-inflammatory macrophages and vSMCs may be responsible for increased CCN2 signaling in the vSMC-enriched medial layer. Although CCN2 is regulated by various cytokines and growth factors at the transcriptional level, TGFβ2 has the most predominant effects on CCN2 expression.[47–49] In this study, we convincingly demonstrate that TGFβ2 released by anti-inflammatory macrophages of IL12p40-deficient mice plays a pathogenic role by increasing the expression of CCN2/MMP2. However, it is not known, if increase in CCN2/MMP2 in vSMCs is solely attributed by

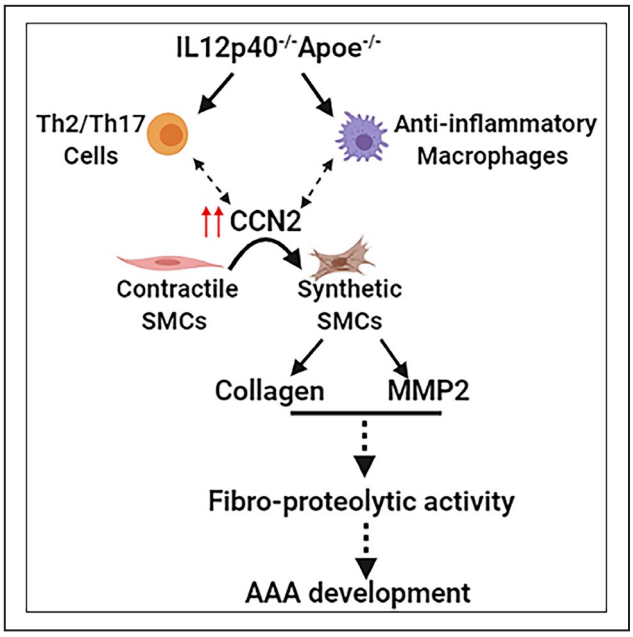

Figure 6. Schematic diagram of the study. The crosstalk between anti-inflammatory macrophages, T cells, and synthetic vascular smooth muscle cell-mediated pathways activate CCN2 (cellular communication network factor 2) signaling leading to increased collagen synthesis and matrix metalloproteinase 2 activity.
These factors predispose the abdominal aorta to abdominal aortic aneurysm in response to angiotensin II.

TGFβ2 derived from *IL12p40*$^{-/-}$*apoE*$^{-/-}$ macrophages. In addition, the molecular mechanism by which these anti-inflammatory macrophages induce CCN2 activation in vSMCs in the setting of AAA needs to be further elucidated. The role of TGFβ signaling in AAA pathogenesis has been shown to be pathogenic, protective, or neutral, depending upon the stage of the disease, the environmental milieu of the vascular injury, and the cell origin.[50–52] Further studies are required to determine if activation of non-canonical pathway of TGFβ2 signaling in the vSMCs is critical to induce CCN2 (Figure 6). It is also possible that crosstalk between vSMCs and T cells play a causative role in the development of AAA in DKO mice. The independent role of vSMCs and Th2/Th17 cytokines in AAA also needs further investigation.

Among the novel genes identified in our protein-array data, betacellulin, a member of the epidermal growth factor family is a potent inducer of synthetic vSMCs leading to proliferation and migration responses in vSMCs.[53] Betacellulin also induces non-canonical TGFβ signaling such as extracellular-signal-regulated kinase 1/2, a serine/threonine protein kinase, and p38 mitogen-activated protein kinase in vSMCs.[54] 4-1BB (CD137) is a potent co-stimulatory molecule that has both immune boosting and immune-suppressing effects.[55] One study reported that 4-1BB exerts a moderate suppressive effect on the progress of autoimmune disease in the absence of IFNγ-mediated signaling.[56] IFNγ is known to inhibit the development of Th17 cells, suggesting that deficiency of IL12p40 may augment AAA by Th17-dependent pathways.[57] While the proinflammatory properties of IL-17 are well known, recent studies have also indicated that IL-17 has anti-inflammatory and profibrotic activities highlighting the Yin and the Yang of most of the cytokines.[58,59] It will be interesting to examine the direct effects of *IL12p40* deficiecy on Th17 cells and its proinflammatory response. Cardiotropin-1 induces cell proliferation, hypertrophy, and secretion of ECM proteins in the vSMC suggesting its role in arterial fibrosis and stiffness, which are features of AAA.[60] In fact, mice lacking cardiotrophin-1 developed less vascular fibrosis with lower deposition of ECM proteins, mainly type I collagen.[61] Infusion of mice with AngII triggers phosphorylation and nuclear translocation of C/EBPβ proteins in aortic cells concomitantly with an increase in the expression of Adamts-1, highlighting the importance of C/EBPβ signaling in AngII-induced upregulation of Adamts-1.[62] Further studies are warranted to investigate the direct roles for these newly identified cytokines in the development of AAA.

The clinical relevance of this study relies in the findings that DKO mice with IL12p40 deficiency may be a better mouse model to study AAA because of its close relevance to human AAA. The predominant and active role of synthetic vSMCs and T cells with IL12p40 deficiency in response to AngII correlated well with the findings observed in human AAA.[38,63] We previously reported the global deficiency of IL12p40 aggravates AngII-induced AAA in the C57BL/6 mice, associated with TGFβ dependent fibrotic mechanism.[17] Interestingly, differential expression of MMP2 was observed in the medial layer of *IL12p40*$^{-/-}$*apoE*$^{-/-}$ (DKO) mice versus adventitial layer in the *IL12p40*$^{-/-}$*apoE*$^{+/+}$ mice. We speculate that this differences could be because of the strain variability (*apoE*$^{+/+}$ *versus apoE*$^{-/-}$) and the distinctive mechanism of AAA development. Further studies are warranted to explore the mechanism of such differential expression. In addition, Yan et al reported that pharmacological modulation of IL12p40 and IL23p19 mitigated elastase-induced AAA by suppressing macrophages expansion and T-cell proliferation.[35] This discrepancy could be because of a complete loss of IL12p40 from birth versus the antagonism of IL12p40 with monoclonal antibody, which may affect macrophage polarization and inflammatory response at various stages of disease progression. Here, we report the activation of TGFβ2/CCN2 signaling pathway in DKO mice at an early stage plays a pathogenic role in AAA. However, in the *apoE*$^{-/-}$ mice, we

speculate that the role of TGFβ2/CCN2 signaling could be a compensatory fibrotic response at a late stage to neutralize the proinflammatory response.

Overall, our studies propose a novel mechanism by which development of AAA is primarily mediated by CCN2/MMP2 pathway. Importantly, these findings suggest that inhibition of IL12 at late stage of the disease with anti-inflammatory drugs may lead to further complications. However, we do not completely ignore the possibility that M2-like macrophages may still be relevant at early stage of the disease to neutralize inflammatory milieu of AAA. On similar lines, it has been shown that blockade of IL12p40 in the early phase of aneurysm development suppresses macrophage expansion, inflammatory cytokine, and MMP9 production and mitigates AAA development.[35] By focusing on a specific cascade of cell-to-cell signaling events in the medial layer of the aorta, future studies will unravel a novel mechanism(s) to understand the pathogenesis of AAA and the critical roles for CCN2 in the modulating synthetic vSMC phenotype.

ARTICLE INFORMATION

Received May 18, 2020; accepted November 16, 2020.

Affiliations

From the Department of Cardiovascular Medicine (N.S., C.P.H.), Dalton Cardiovascular Research Center (N.S., C.P.H.) and Department of Medical Pharmacology and Physiology, University of Missouri, Columbia, MO (C.P.H.).

Acknowledgments

The authors thank Dr. Helena Kuivaniemi for providing the human AAA and non-AAA aortic specimens for the immunohistochemistry and laser capture microdissection studies, and for a critical review of the article. The authors thank Dr. Zhe Sun at imaging core facility at Dalton Cardiovascular Research Center for capturing the ultrasound images. We thank Dr. Christine Pham and Dr. Huimin Yan for the technical support with elastase infusion method of AAA. We also thank Dr. Annayya Aroor for the atomic force microscopy-related experiments.

Sources of Funding

This work was supported by National Institutes of Health Grant R01HL124155 (C.P.H.), Veterans Affairs Merit grant (1I01BX002714; Christine Pham), and funding from the University of Missouri to C.P.H. Collection of human tissue samples was funded by a grant from the National Heart, Lung, and Blood Institute (HL064310 to H. Kuivaniemi).

Disclosures

None.

Supplementary Material

Data S1
Tables S1–S3
Figures S1–S9

REFERENCES

1. Benjamin EJ, Virani SS, Callaway CW, Chamberlain AM, Chang AR, Cheng S, Chiuve SE, Cushman M, Delling FN, Deo R, et al. Heart disease and stroke statistics—2018 update: A report from the american heart association. *Circulation*. 2018;137:e67–e492.
2. Parisi L, Gini E, Baci D, Tremolati M, Fanuli M, Bassani B, Farronato G, Bruno A, Mortara L. Macrophage polarization in chronic inflammatory diseases: Killers or builders? *Journal of Immunology Research*. 2018;2018:25. DOI: 10.1155/2018/8917804.
3. Raffort J, Lareyre F, Clément M, Hassen-Khodja R, Chinetti G, Mallat Z. Monocytes and macrophages in abdominal aortic aneurysm. *Nat Rev Cardiol*. 2017;14:457. DOI: 10.1038/nrcardio.2017.52.
4. Hans CP, Koenig SN, Huang N, Cheng J, Beceiro S, Guggilam A, Kuivaniemi H, Partida-Sanchez S, Garg V. Inhibition of notch1 signaling reduces abdominal aortic aneurysm in mice by attenuating macrophage-mediated inflammation. *Arterioscler Thromb Vasc Biol*. 2012;32:3012–3023. DOI: 10.1161/ATVBAHA.112.254219.
5. Rateri DL, Howatt DA, Moorleghen JJ, Charnigo R, Cassis LA, Daugherty A. Prolonged infusion of angiotensin ii in apoe(-/-) mice promotes macrophage recruitment with continued expansion of abdominal aortic aneurysm. *Am J Pathol*. 2011;179:1542–1548. DOI: 10.1016/j.ajpath.2011.05.049.
6. Daugherty A, Manning MW, Cassis LA. Angiotensin ii promotes atherosclerotic lesions and aneurysms in apolipoprotein e-deficient mice. *J Clin Invest*. 2000;105:1605–1612. DOI: 10.1172/JCI7818.
7. Miyake T, Morishita R. Pharmacological treatment of abdominal aortic aneurysm. *Cardiovasc Res*. 2009;83:436–443. DOI: 10.1093/cvr/cvp155.
8. Baxter BT, Terrin MC, Dalman RL. Medical management of small abdominal aortic aneurysms. *Circulation*. 2008;117:1883–1889. DOI: 10.1161/CIRCULATIONAHA.107.735274.
9. Dale MA, Ruhlman MK, Baxter BT. Inflammatory cell phenotypes in aaas; their role and potential as targets for therapy. *Arterioscler Thromb Vasc Biol*. 2015;35:1746–1755. DOI: 10.1161/ATVBAHA.115.305269.
10. Wilson WRW, Wills J, Furness PN, Loftus IM, Thompson MM. Abdominal aortic aneurysm rupture is not associated with an up-regulation of inflammation within the aneurysm wall. *Eur J Vasc Endovasc Surg*. 2010;40:191–195. DOI: 10.1016/j.ejvs.2010.04.014.
11. Lindeman JH, Rabelink TJ, van Bockel JH. Immunosuppression and the abdominal aortic aneurysm: Doctor jekyll or mister hyde? *Circulation*. 2011;124:e463–465. DOI: 10.1161/CIRCULATIONAHA.110.008573.
12. Meijer CA, Stijnen T, Wasser MNJM, Hamming JF, van Bockel JH, Lindeman JHN, et al. Doxycycline for stabilization of abdominal aortic aneurysms: A randomized trial. *Ann Intern Med*. 2013;159:815–823. DOI: 10.7326/0003-4819-159-12-201312170-00007.
13. Xie X, Lu H, Moorleghen JJ, Howatt DA, Rateri DL, Cassis LA, Daugherty A. Doxycycline does not influence established abdominal aortic aneurysms in angiotensin ii-infused mice. *PLoS One*. 2012;7:e46411. DOI: 10.1371/journal.pone.0046411.
14. Cheng Z, Zhou Y-Z, Wu Y, Wu Q-Y, Liao X-B, Fu X-M, Zhou X-M. Diverse roles of macrophage polarization in aortic aneurysm: Destruction and repair. *J Transl Med*. 2018;16:354. DOI: 10.1186/s12967-018-1731-0.
15. Mantovani A, Sica A, Sozzani S, Allavena P, Vecchi A, Locati M. The chemokine system in diverse forms of macrophage activation and polarization. *Trends Immunol*. 2004;25:677–686. DOI: 10.1016/j.it.2004.09.015.
16. Bastos KRB, Alvarez JM, Marinho CRF, Rizzo LV, Lima MRD. Macrophages from il-12p40-deficient mice have a bias toward the m2 activation profile. *J Leukoc Biol*. 2002;71:271–278.
17. Sharma N, Dev R, Belenchia AM, Aroor AR, Whaley-Connell A, Pulakat L, Hans CP. Deficiency of il12p40 (interleukin 12 p40) promotes ang ii (angiotensin ii)-induced abdominal aortic aneurysm. *Arterioscler Thromb Vasc Biol*. 2019;39:212–223. DOI: 10.1161/ATVBAHA.118.311969.
18. Wills-Karp M. Il-12/il-13 axis in allergic asthma. *Journal of Allergy and Clinical Immunology*. 2001;107:9–18. DOI: 10.1067/mai.2001.112265.
19. Dickensheets HL, Freeman SL, Donnelly RP. Interleukin-12 differentially regulates expression of ifn-γ and interleukin-2 in human t lymphoblasts. *J Interferon Cytokine Res*. 2000;20:897–905. DOI: 10.1089/10799900050163271.
20. Villarino AV, Tato CM, Stumhofer JS, Yao Z, Cui YK, Hennighausen L, O'Shea JJ, Hunter CA. Helper t cell il-2 production is limited by negative feedback and stat-dependent cytokine signals. *J Exp Med*. 2007;204:65–71. DOI: 10.1084/jem.20061198.
21. Gong D, Shi W, Yi SJ, Chen H, Groffen J, Heisterkamp N. Tgfbeta signaling plays a critical role in promoting alternative macrophage activation. *BMC Immunol*. 2012;13:31.
22. Li MO, Wan YY, Sanjabi S, Robertson AK, Flavell RA. Transforming growth factor-beta regulation of immune responses. *Annu Rev Immunol*. 2006;24:99–146.
23. Hoshina K, Koyama H, Miyata T, Shigematsu H, Takato T, Dalman RL, Nagawa H. Aortic wall cell proliferation via basic fibroblast growth factor gene transfer limits progression of experimental abdominal aortic aneurysm. *J Vasc Surg*. 2004;40:512–518. DOI: 10.1016/j.jvs.2004.06.018.

24. Humphrey JD, Milewicz DM. Aging, smooth muscle vitality, and aortic integrity. *Circ Res*. 2017;120:1849–1851. DOI: 10.1161/CIRCRESAHA.117.311075.
25. Ailawadi G, Moehle CW, Pei H, Walton SP, Yang Z, Kron IL, Lau CL, Owens GK. Smooth muscle phenotypic modulation is an early event in aortic aneurysms. *J Thorac Cardiovasc Surg*. 2009;138:1392–1399. DOI: 10.1016/j.jtcvs.2009.07.075.
26. Raines EW, Ross R. Smooth muscle cells and the pathogenesis of the lesions of atherosclerosis. *Br Heart J*. 1993;69:S30–37. DOI: 10.1136/hrt.69.1_Suppl.S30.
27. Petsophonsakul P, Furmanik M, Forsythe R, Dweck M, Schurink GW, Natour E, Reutelingsperger C, Jacobs M, Mees B, Schurgers L. Role of vascular smooth muscle cell phenotypic switching and calcification in aortic aneurysm formation. *Arterioscler Thromb Vasc Biol*. 2019;39:1351–1368. DOI: 10.1161/ATVBAHA.119.312787.
28. Davis FM, Rateri DL, Balakrishnan A, Howatt DA, Strickland DK, Muratoglu SC, Haggerty CM, Fornwalt BK, Cassis LA, Daugherty A. Smooth muscle cell deletion of low-density lipoprotein receptor-related protein 1 augments angiotensin ii-induced superior mesenteric arterial and ascending aortic aneurysms. *Arterioscler Thromb Vasc Biol*. 2015;35:155–162. DOI: 10.1161/ATVBAHA.114.304683.
29. Airhart N, Brownstein BH, Cobb JP, Schierding W, Arif B, Ennis TL, Thompson RW, Curci JA. Smooth muscle cells from abdominal aortic aneurysms are unique and can independently and synergistically degrade insoluble elastin. *J Vasc Surg*. 2014;60(1033–1041):discussion 1041–1032. DOI: 10.1016/j.jvs.2013.07.097.
30. Perbal B, Tweedie S, Bruford E. The official unified nomenclature adopted by the hgnc calls for the use of the acronyms, ccn1–6, and discontinuation in the use of cyr61, ctgf, nov and wisp 1–3 respectively. *Journal of Cell Communication and Signaling*. 2018;12:625–629. DOI: 10.1007/s12079-018-0491-1.
31. Mazzocca A, Fransvea E, Dituri F, Lupo L, Antonaci S, Giannelli G. Down-regulation of connective tissue growth factor by inhibition of transforming growth factor betablocks the tumor-stroma cross-talk and tumor progression in hepatocellular carcinoma. *Hepatology*. 2010;51:523–534.
32. Abraham D. Connective tissue growth factor: Growth factor, matricellular organizer, fibrotic biomarker or molecular target for anti-fibrotic therapy in ssc? *Rheumatology (Oxford)*. 2008;47(Suppl 5):v8–9. DOI: 10.1093/rheumatology/ken278.
33. Sharma N, Dev R, Ruiz-Rosado JDD, Partida-Sanchez S, Guerau-de-Arellano M, Dhakal P, Kuivaniemi H, Hans CP. Pharmacological inhibition of notch signaling regresses pre-established abdominal aortic aneurysm. *Sci Rep*. 2019;9(13458). DOI: 10.1038/s41598-019-49682-0.
34. Robinet P, Milewicz DM, Cassis LA, Leeper NJ, Lu HS, Smith JD. Consideration of sex differences in design and reporting of experimental arterial pathology studies-statement from atvb council. *Arterioscler Thromb Vasc Biol*. 2018;38:292–303. DOI: 10.1161/ATVBAHA.117.309524.
35. Yan H, Hu Y, Akk A, Ye K, Bacon J, Pham CTN. Interleukin-12 and -23 blockade mitigates elastase-induced abdominal aortic aneurysm. *Sci Rep*. 2019;9:10447. DOI: 10.1038/s41598-019-46909-y.
36. Sharma N, Sun Z, Hill MA, Hans CP. Measurement of pulse propagation velocity, distensibility and strain in an abdominal aortic aneurysm mouse model. *J Vis Exp*. 2020:e60515. DOI: 10.3791/60515.
37. Lillvis JH, Erdman R, Schworer CM, Golden A, Derr K, Gatalica Z, Cox LA, Shen J, Vander Heide RS, Lenk GM, et al. Regional expression of hoxa4 along the aorta and its potential role in human abdominal aortic aneurysms. *BMC Physiol*. 2011;11:9. DOI: 10.1186/1472-6793-11-9.
38. Sagan A, Mikolajczyk TP, Mrowiecki W, MacRitchie N, Daly K, Meldrum A, Migliarino S, Delles C, Urbanski K, Filip G, et al. T cells are dominant population in human abdominal aortic aneurysms and their infiltration in the perivascular tissue correlates with disease severity. *Front Immunol*. 2019;10:1979. DOI: 10.3389/fimmu.2019.01979.
39. Téo FH, de Oliveira RTD, Villarejos L, Mamoni RL, Altemani A, Menezes FH, Blotta M. Characterization of cd4(+) t cell subsets in patients with abdominal aortic aneurysms. *Mediators Inflamm*. 2018;2018:6967310.
40. Tesmer LA, Lundy SK, Sarkar S, Fox DA. Th17 cells in human disease. *Immunol Rev*. 2008;223:87–113. DOI: 10.1111/j.1600-065X.2008.00628.x.
41. Sachdeva J, Mahajan A, Cheng J, Baeten JT, Lilly B, Kuivaniemi H, Hans CP. Smooth muscle cell-specific notch1 haploinsufficiency restricts the progression of abdominal aortic aneurysm by modulating ctgf expression. *PLoS One*. 2017;12:e0178538. DOI: 10.1371/journal.pone.0178538.
42. Liu J, Cao S, Kim S, Chung EY, Homma Y, Guan X, Jimenez V, Ma X. Interleukin-12: An update on its immunological activities, signaling and regulation of gene expression. *Curr Immunol Rev*. 2005;1:119–137.
43. Saraff K, Babamusta F, Cassis LA, Daugherty A. Aortic dissection precedes formation of aneurysms and atherosclerosis in angiotensin ii-infused, apolipoprotein e-deficient mice. *Arterioscler Thromb Vasc Biol*. 2003;23:1621–1626. DOI: 10.1161/01.ATV.0000085631.76095.64.
44. Friedrichsen S, Heuer H, Christ S, Cuthill D, Bauer K, Raivich G. Gene expression of connective tissue growth factor in adult mouse. *Growth Factors*. 2005;23:43–53. DOI: 10.1080/08977190512331340566.
45. Middleton RK, Lloyd GM, Bown MJ, Cooper NJ, London NJ, Sayers RD. The pro-inflammatory and chemotactic cytokine microenvironment of the abdominal aortic aneurysm wall: A protein array study. *J Vasc Surg*. 2007;45:574–580. DOI: 10.1016/j.jvs.2006.11.020.
46. Szekanecz Z, Shah MR, Pearce WH, Koch AE. Human atherosclerotic abdominal aortic aneurysms produce interleukin (il)-6 and interferon-gamma but not il-2 and il-4: The possible role for il-6 and interferon-gamma in vascular inflammation. *Agents Actions*. 1994;42:159–162. DOI: 10.1007/BF01983484.
47. Fan W-H, Pech M, Karnovsky MJ. Connective tissue growth factor (ctgf) stimulates vascular smooth muscle cell growth and migration in vitro. *Eur J Cell Biol*. 2000;79:915–923. DOI: 10.1078/0171-9335-00122.
48. Dituri F, Cossu C, Mancarella S, Giannelli G. The interactivity between tgfβ and bmp signaling in organogenesis, fibrosis, and cancer. *Cells*. 2019;8:1130. DOI: 10.3390/cells8101130.
49. Klaassen I, van Geest RJ, Kuiper EJ, van Noorden CJF, Schlingemann RO. The role of ctgf in diabetic retinopathy. *Exp Eye Res*. 2015;133:37–48. DOI: 10.1016/j.exer.2014.10.016.
50. Daugherty A, Chen Z, Sawada H, Rateri DL, Sheppard MB. Transforming growth factor-β in thoracic aortic aneurysms: Good, bad, or irrelevant? *Journal of the American Heart Association: Cardiovascular and Cerebrovascular Disease*. 2017;6:e005221. DOI: 10.1161/JAHA.116.005221.
51. Akhurst RJ. The paradoxical tgf-beta vasculopathies. *Nat Genet*. 2012;44:838–839.
52. Lin FY, Yang XA. Tgf-beta signaling in aortic aneurysm: Another round of controversy. *Journal of Genetics and Genomics*. 2010;37:583–591.
53. Zhang D, Shen B, Zhang Y, Ni N, Wang Y, Fan X, Sun H, Gu P. Betacellulin regulates the proliferation and differentiation of retinal progenitor cells in vitro. *J Cell Mol Med*. 2018;22:330–345.
54. Akhtar S, Yousif MHM, Chandrasekhar B, Benter IF. Activation of egfr/erbb2 via pathways involving erk1/2, p38 mapk, akt and foxo enhances recovery of diabetic hearts from ischemia-reperfusion injury. *PLoS One*. 2012;7:e39066. DOI: 10.1371/journal.pone.0039066.
55. Chu D-T, Bac ND, Nguyen K-H, Tien NLB, Thanh VV, Nga VT, Ngoc VTN, Anh Dao DT, Hoan LN, Hung NP, et al. An update on anti-cd137 antibodies in immunotherapies for cancer. *Int J Mol Sci*. 2019;20:1822. DOI: 10.3390/ijms20081822.
56. Kim YH, Choi BK, Shin SM, Kim CH, Oh HS, Park SH, Lee DG, Lee MJ, Kim KH, Vinay DS, et al. 4–1bb triggering ameliorates experimental autoimmune encephalomyelitis by modulating the balance between th17 and regulatory t cells. *J Immunol*. 2011;187:1120. DOI: 10.4049/jimmunol.1002681.
57. Yeh W-I, McWilliams IL, Harrington LE. Ifnγ inhibits th17 differentiation and function via tbet-dependent and tbet-independent mechanisms. *J Neuroimmunol*. 2014;267:20–27. DOI: 10.1016/j.jneuroim.2013.12.001.
58. Ke Y, Liu K, Huang G-Q, Cui Y, Kaplan HJ, Shao H, Sun D. Anti-inflammatory role of il-17 in experimental autoimmune uveitis. *Journal of immunology (Baltimore, Md*. 1950;2009(182):3183–3190.
59. Amatya N, Garg AV, Gaffen SL. Il-17 signaling: The yin and the yang. *Trends Immunol*. 2017;38:310–322. DOI: 10.1016/j.it.2017.01.006.
60. Lopez-Andres N, Fortuno MA, Diez J, Zannad F, Lacolley P, Rossignol P. Vascular effects of cardiotrophin-1: A role in hypertension? *J Hypertens*. 2010;28:1261–1272. DOI: 10.1097/HJH.0b013e328337fe42.
61. López-Andrés N, Calvier L, Labat C, Fay R, Díez J, Benetos A, Zannad F, Lacolley P, Rossignol P. Absence of cardiotrophin 1 is associated with decreased age-dependent arterial stiffness and increased longevity in mice. *Hypertension*. 2013;61:120–129. DOI: 10.1161/HYPERTENSIONAHA.112.201699.
62. Oller J, Alfranca A, Méndez-Barbero N, Villahoz S, Lozano-Vidal N, Martín-Alonso M, Arroyo AG, Escolano A, Armesilla AL, Campanero MR, et al. C/ebpβ and nuclear factor of activated t cells differentially regulate adamts-1 induction by stimuli associated with vascular remodeling. *Mol Cell Biol*. 2015;35:3409–3422. DOI: 10.1128/MCB.00494-15.
63. Petsophonsakul P, Furmanik M, Forsythe R, Dweck M, Schurink Geert W, Natour E, Reutelingsperger C, Jacobs M, Mees B, Schurgers L. Role of vascular smooth muscle cell phenotypic switching and calcification in aortic aneurysm formation. *Arterioscler Thromb Vasc Biol*. 2019;39:1351–1368. DOI: 10.1161/ATVBAHA.119.312787.

SUPPLEMENTAL MATERIAL

Data S1. Major Resources Tables.

Animals (in vivo studies)

Species	Vendor or Source	Background Strain	Sex
Il12p40$^{-/-}$ mice	The Jackson Laboratory	C57BL/6J	M
Apoe$^{-/-}$ mice	The Jackson Laboratory	C57BL/6J	M
Ccn2$^{+/-}$ mice	The Jackson Laboratory	129S6/C57BL/6J	M

Animal breeding

	Species	Vendor or Source	Background Strain	Other Information
Parent - Male	*Il12p40*$^{-/-}$ mice	The Jackson Laboratory	C57BL/6J	The heterozygote pups obtained from these breeders were further bred to obtain *IL12p40*$^{-/-}$*Apoe*$^{-/-}$ and *Apoe*$^{-/-}$ littermates.
Parent - Female	*Apoe*$^{-/-}$ mice	The Jackson Laboratory	C57BL/6J	
Parent - Male	*Ccn2*$^{+/-}$ mice	The Jackson Laboratory	129S6	The *Ccn2*$^{+/-}$ mice and their *Ccn2*$^{+/+}$ littermate mice generated from these breeders after ~6 backcrosses with WT (C57BL/6J) mice were used.
Parent - Female	*Ccn2*$^{+/-}$ mice	The Jackson Laboratory	129S6	

Antibodies

Target antigen	Vendor or Source	Catalog #	Working concentration	Lot # (preferred but not required)
F4/80	Abcam	ab100790	1:200	
IFNγ	Abcam	ab9657	1:400	
CD3	Abcam	ab5690	1:200 for IHC and DIF	
IL17	Abcam	ab79056	1:400	
Tgfβ2	Abcam	ab36495	1:200 for IHC 1:2,000 for WB	
Tgfβ1	Abcam	ab92486	1:2,000 for WB	
Mmp2	Abcam	ab97779	1:200 for IHC 1:2,000 for WB	
CCN2	Abcam	ab6992	1:200 for IHC 1:2,000 for WB	
Smoothelin B	Abcam	ab204305	1:400 for IHC	
active caspase-3	Cell signaling	9661S	1:200 for IHC	
CEBPβ	Cell signaling	sc-7962	1:200 for DIF	
GAPDH	Novus Biologicals	NB300-221	1:5,000 for WB	
β-actin	Abcam	ab8226	1:10,000 for WB	

Cultured Cells

Name	Vendor or Source	Sex (F, M, or unknown)
Human aortic smooth muscle cells (HaSMCs)	Lonza (CC-2571)	Unknown
Mouse vSMCs	Primary cells isolated from the abdominal aorta of mice	Male mice
Mouse Fibroblasts (MEF)	Primary cells isolated from mice embryos	Male mice
Macrophages (RAW Cells 264.7)	ATCC	Unknown

Table S1. List of human primer sequences used for qRT-PCR studies.

Gene	Forward Primer (5'-3')	Reverse Primer (5'-3')
MMP2	ACG ACC GCG ACA AGA AGT AT	ATT TGT TGC CCA GGA AAG TG
OPN	GCC GAG GTG ATA GTG TGG TT	ACG GCT GTC CCA ATC AGA AG
MMP9	GAC AAG CTC TTC GGC TTC TG	TCG CTG GTA CAG GTC GAG TA
CCN2	CTC CAC CCG GGT TAC CAA TG	CCG GGA CAG TTG TAA TGG CA
TGFß1	CCT ACT TCT GCA CGA TGT GAT G	CCT TTG CTA CGG TTG GTT ACA TT
TGFß2	AAA GCC AGA GTG CCT GAA CA	AGC GCT GGG TTG GAG ATG
SMB	GAG ATT GAG GCT GCC ACC TT	GCT TTG AAA CCT CTG CCT GC
COL1A1	CAG CCG CTT CAC CTA CAG C	TTT TGT ATT CAA TCA CTG TCT TGC C

Table S2. List of primer sequences used for qRT-PCR studies for Mus musculus.

Gene	Forward Primer (5'-3')	Reverse Primer (5'-3')
Il12p40	CAC CTG TGA CAC GCC TGA AG	CTC AGA GTC TCG CCT CCT TT
Il23p19	CCC ATG GAG CAA CTT CAC AC	GCT GCC ACT GCT GAC TAG AAC
Il10	CAC TGC TAT GCT GCC TGC TC	TGG CCT TGT AGA CAC CTT GG
Roryt	GCA GCG CTC CAA CAT CTT CT	ACG TAC TGA ATG GCC TCG GT
Foxp3	CAC CTG GCT GGG AAA ATG G	GGA GCC CTT GTC GGA TGA
Tnfα	CCC ACT CTG ACC CCT TTA CT	TTT GAG TCC TTG ATG GTC GT
Cebpß	GGT TTC GGG ACT TGA TGC A	CAA CAA CCC CGC AGG AAC
Il17a	TCC CCT CTG TGA TCT GGG AAG	AGC ATC TTC TCG ACC CTG AA
Il17f	CTG GAG GAT AAC ACT GTG AGA GT	TGC TGA ATG GCG ACG GAG TTC
Il18	CAG GCC TGA CAT CTT CTG CAA	CTG ACA TGG CAG CCA TTG T
Ifng	ATG AAC GCT ACA CAC TGC ATC	CCA TCC TTT TGC CAG TTC CTC
Tgfß2	AGA ATC GTC CGC TTT GAT GTC TC	ATA CAG TTC AAT CCG CTG CTC G
Cd206	CAGGTGTGGGCTCAGGTAGT	TGTGGTGAGCTGAAAGGTGA
Mmp2	GAT GTC GCC CCT AAA ACA GA	TGG TGT TCT GGT CAA GGT CA
Il4	ATT TTG AAC GAG GTC ACA GGA GAA G	ACC TTG GAA GCC CTA CAG ACG AG
Mmp9	AGA CCT GAA AAC CTC CAA CCT CAC	TGT TAT GAT GGT CCC ACT TGA GGC
Stat6	CTG GGG TGG TTT CCT CTT G	TGC CCG GTC TCA CCT AAC TA
Smad2	CTT GAT GGC CGT CTT CAG GT	CCA GAA TGC AGG TTC CGA GT
Smad3	GAG GAG AAG TGG TGC GAG AAG	TGG GGA TGG TAA TGC ACT TGG
Tgfß1	AAG TTG GCA TGG TAG CCC TT	GCC CTG GAT ACC AAC TAT TGC
Il17	ATC CCT CAA AGC TCA GCG TGT C	GGG TCT TCA TTG CGG TGG AGA G
Ccn2	CTT CTG CGA TTT CGG CTC C	TGC TTT GGA AGG ACT CAC CG
Il6	CTA CCC CAA TTT CCA ATG CT	ACC ACA GTG AGG AAT GTC CA

Table S3. **Full names of proteins (abbreviations listed in Table 1).**

Protein Abbr.	**Protein name**
Ang-3	Angiopoietin-like 3
4-1BB/TNFRSF9	TNF-receptor superfamily 9
Il-22	Interleukin 22
Il-17F	Interleukin 17F
Prl	Prolactin
Il-20	Interleukin 20
Il-17E	Interleukin 17E
Il-2Ra	Interleukin 2R alpha
CD-27/ TNFRSF7	Tumor necrosis factor receptor superfamily 7
Taci	Transmembrane activator and CAML interactor
Il-7Ra	Interleukin-7 receptor subunit alpha
Il-13	Interleukin 13
Cd-40L	CD40 ligand
Alk-1	Activin receptor-like kinase 1
Adamts-1	ADAM Metallopeptidase With Thrombospondin Type 1 Motif 1
Ct-1	Cardiotrophin-1
Vegf-B	Vascular endothelial growth factor B
Mfg-e8	Milk fat globule-EGF factor 8
VEGF R1	Vascular permeability factor receptor 1
Shh-N	Sonic Hedgehog
Mmp-10	Metalloproteinase-10
Nov/Ccn3	Nephroblastoma
IL-1ra	Interleukin-1 receptor antagonist
Mcp-1	Monocyte chemoattractant protein-1
Kc	Keratinocytes-derived chemokine
m-Csf	Macrophage colony-stimulating factor
Mip-2	Macrophage Inflammatory Proteins
Tnf-α	Tumor necrosis factor alpha
Igfbp-3	Insulin-like growth factor binding protein 3
Sdf-1α	Stromal cell-derived factor 1 alpha
Lix	C-X-C motif chemokine 5
Il-6	Interleukin 6
Crp	C-reactive protein
Gm-Csf	Granulocyte Macrophage Colony-Stimulating Factor

Figure S1. (A and B), Pictures of aortae from the dead mice showing acute dissection in *Apoe*$^{-/-}$ and DKO mice in response to AngII. (C-F), Representative images of the thoracic aorta from experimental mice at day 28. Scale bar = 1 mm.

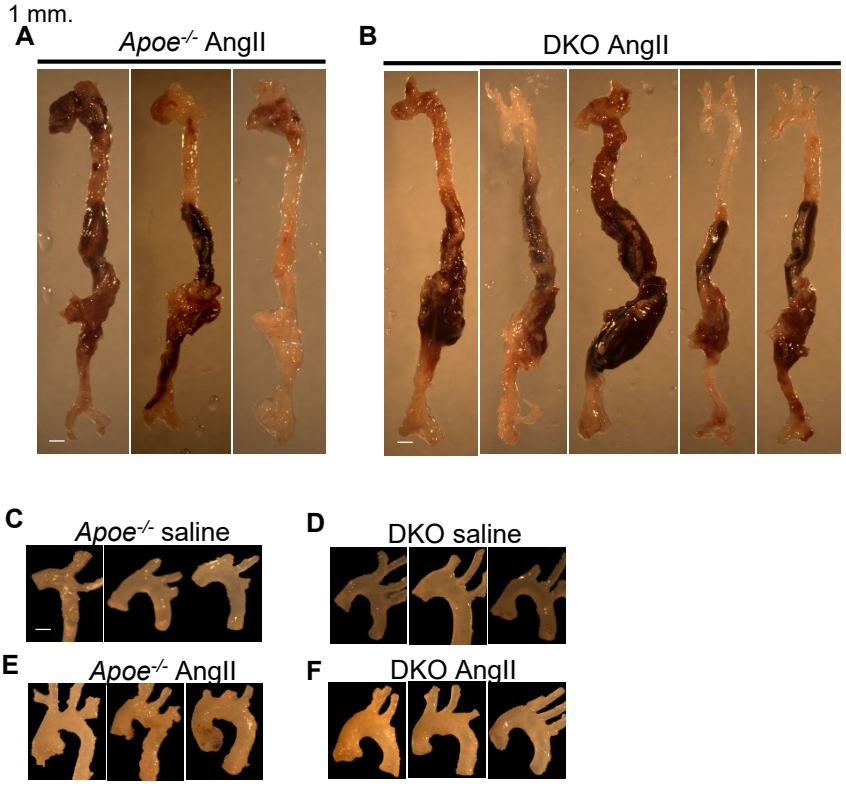

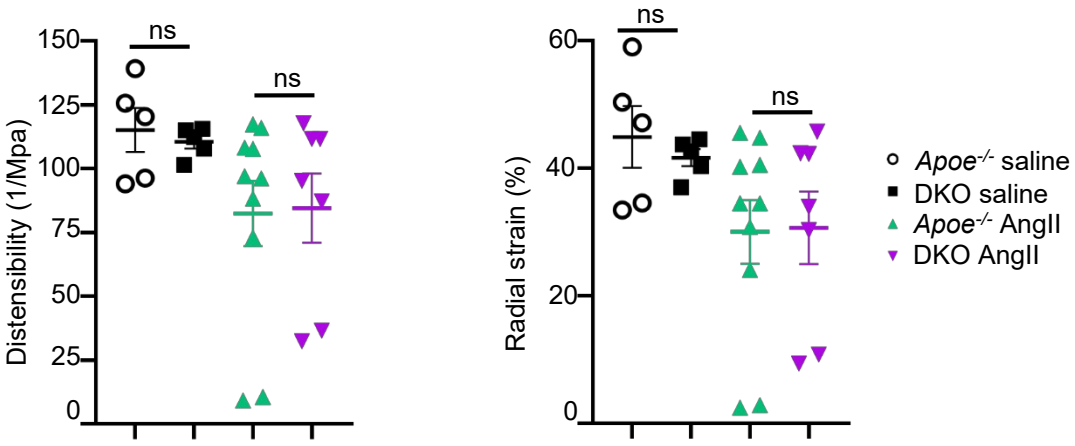

Figure S2. **Distensibility and radial strain calculated from measurements of abdominal aortic pulse pressure as determined by EKV in response to AngII at day 28 as measured by Vevo Vasc analysis (n=6; saline and n=12; AngII).** ns = non-significant.

Figure S3. Caspase 3 immunostaining in the aortic tissue of *Apoe*$^{-/-}$ and DKO mice at day 28 of AngII infusion. Scale bar = 50 μm.

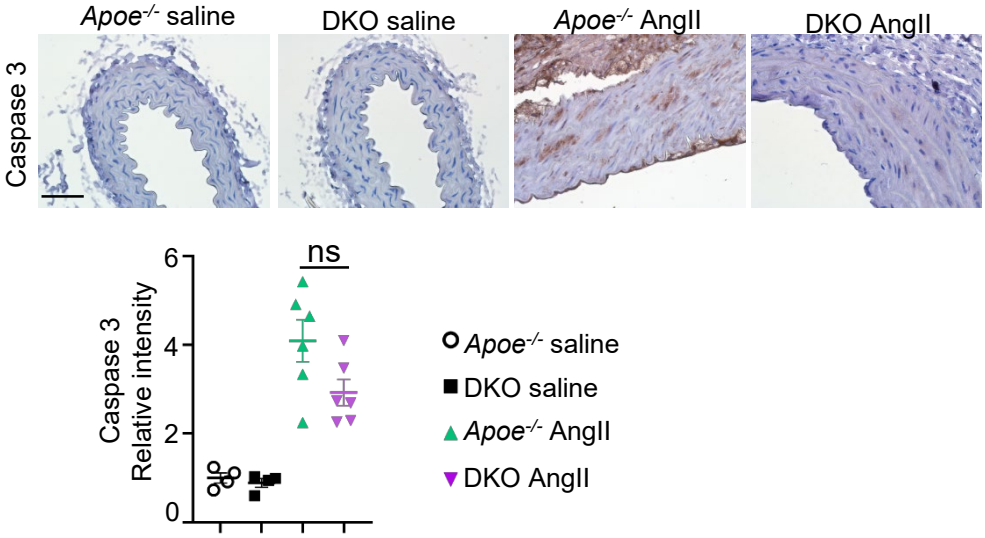

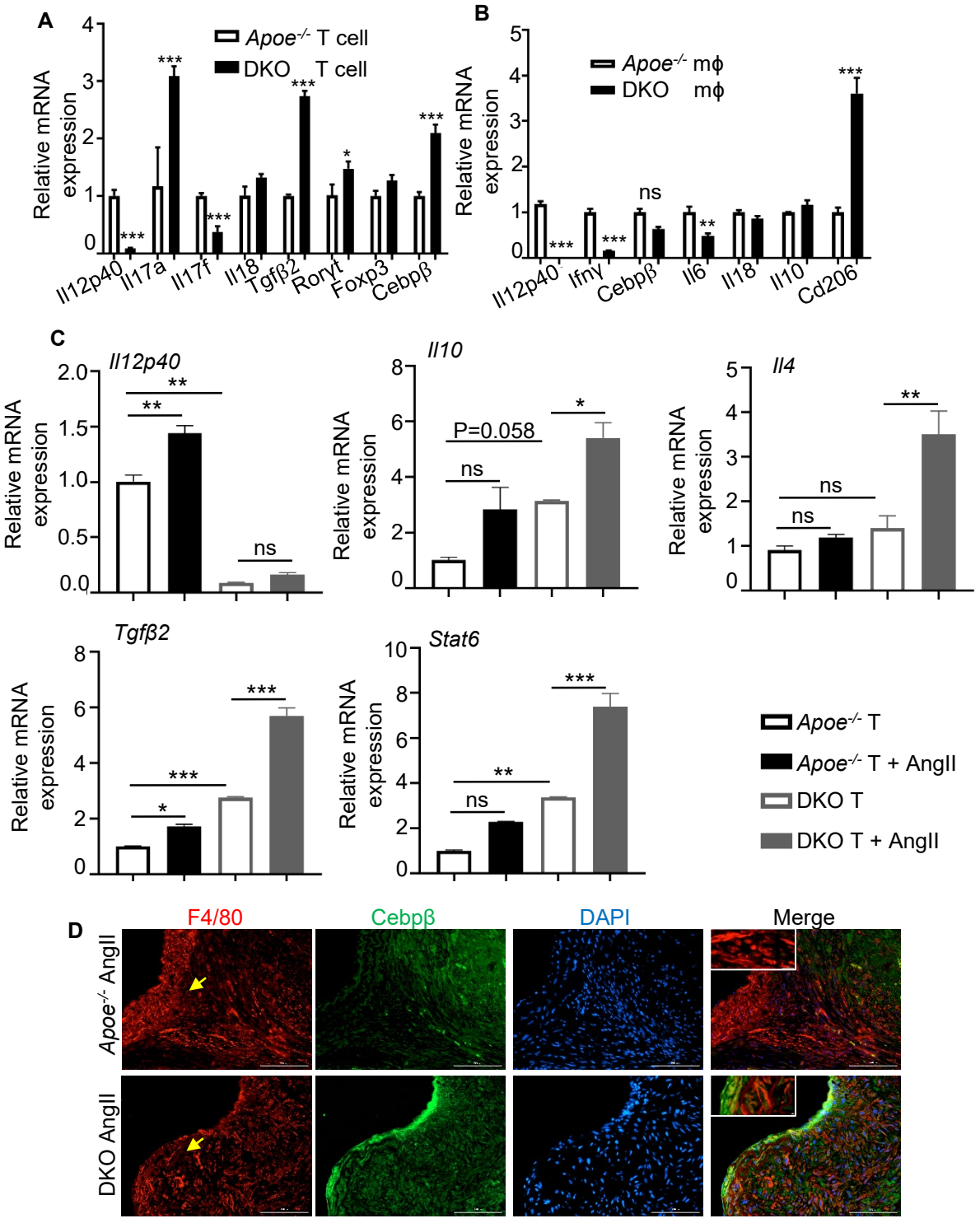

Figure S4. (A and B), mRNA expression of various cytokines in T cells and macrophages (mϕ) isolated from *Apoe*$^{-/-}$ and DKO mice. (C), mRNA expression of *Il12p40*, *Il10*, *Il4*, *Tgfβ2* and *Stat6* in the T cell isolated from spleen of *Apoe*$^{-/-}$ and DKO mice and treated with or without AngII (n=3; saline and n=4; AngII). (D), F4/80 and Cebpβ expression and their weak co-localization in the aortic tissues from AngII-infused *Apoe*$^{-/-}$ and DKO mice. Yellow arrows in **D** represent elastin breaks. *P<0.05; **P<0.01; ***P<0.001 by paired two-tailed Student's t-test.

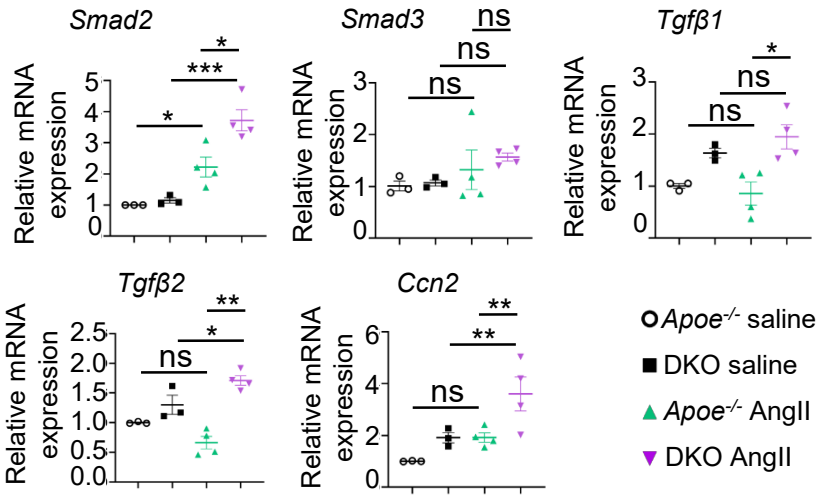

Figure S5. mRNA expression of CCN2 associated genes in the aortic tissues of *Apoe*$^{-/-}$ and DKO mice at day 28 of AngII infusion (n=3; saline and n=4; AngII).

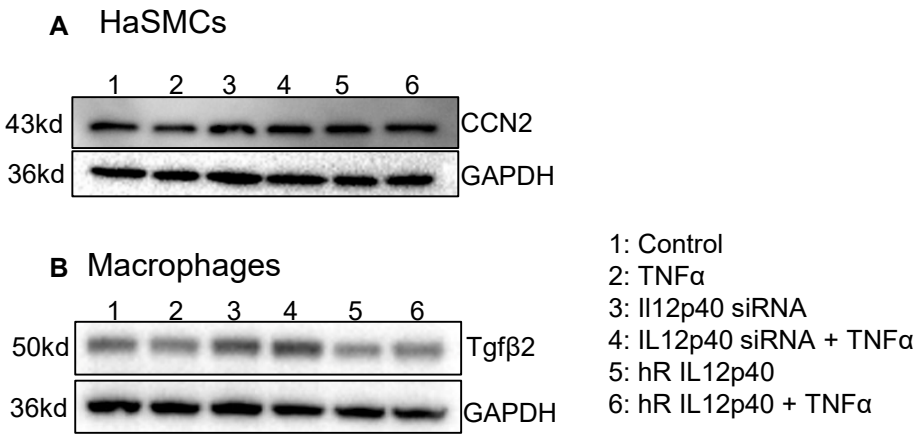

Figure S6. (A and B), Western blot showing expression of CCN2 (A), Tgfβ2 (B) and GAPDH as housekeeping genes in the human aortic SMCs (A) and macrophages (B) treated with IL12p40 siRNA and recombinant human IL12p40 protein.

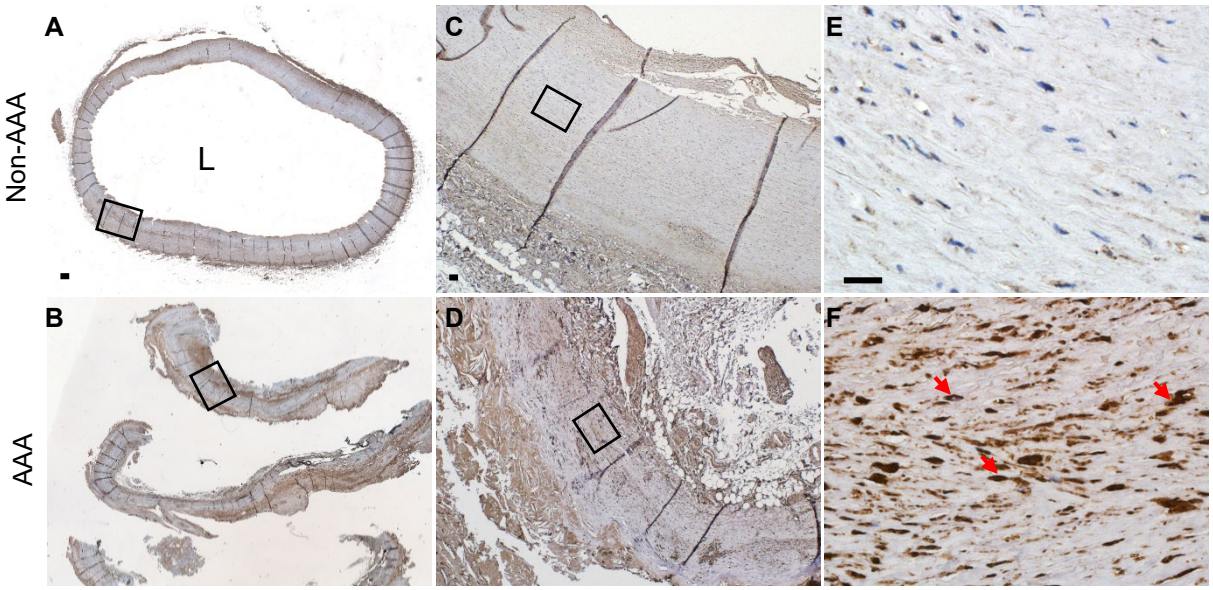

Figure S7. **Differential expression of CCN2 immunostaining in the media and adventitia of human AAA as shown by IHC. (A and B), montage images of aortic section.** Scale bar = 50 mm in A-B; = 1 mm in C-D and 50 μm in E-F. L= lumen (n=6).

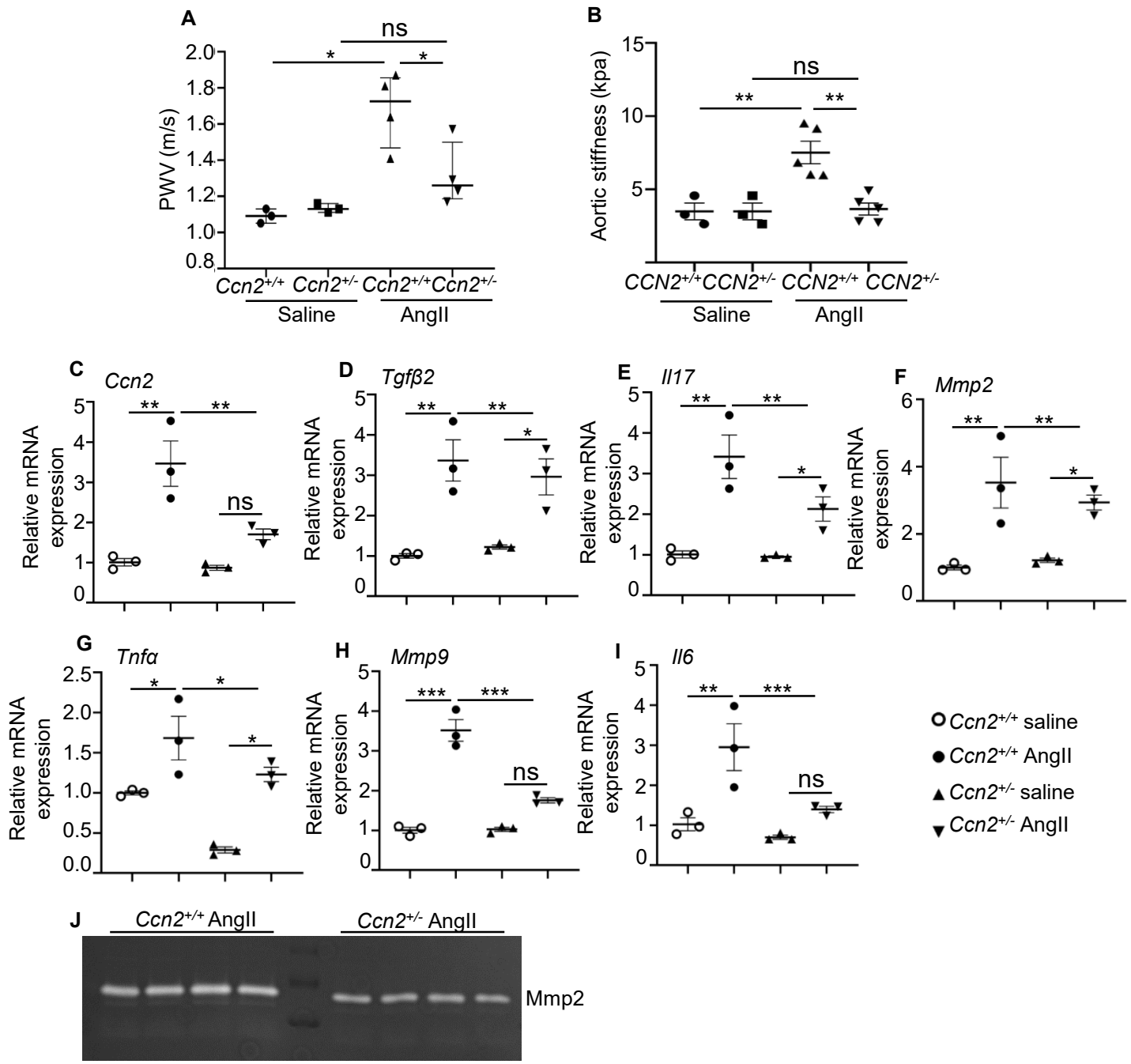

Figure S8. **Ccn2 deficiency decreases aortic stiffness of the aorta.** (**A**), Pulse-wave velocity (PWV) calculated from measurements of abdominal aortic pulse pressure as determined by EKV in response to AngII at day 7 (n=3 for control and 4 for AngII). (**B**), Abdominal aortic stiffness as measured by atomic force microscopy at day 7 of AngII infusion in experimental mice. (**C-I**), Gene expression of various cytokines in the aortic tissues of experimental mice at day 7 of saline or AngII infusion. (**J**), Gelatin zymography showing MMP2 activity on aortic samples derived from AngII-infused *CCN2*$^{+/+}$ and *CCN2*$^{+/-}$ mice. *p<0.05, **p<0.01, ***p<0.001 in Tukey's multiple comparisons test.

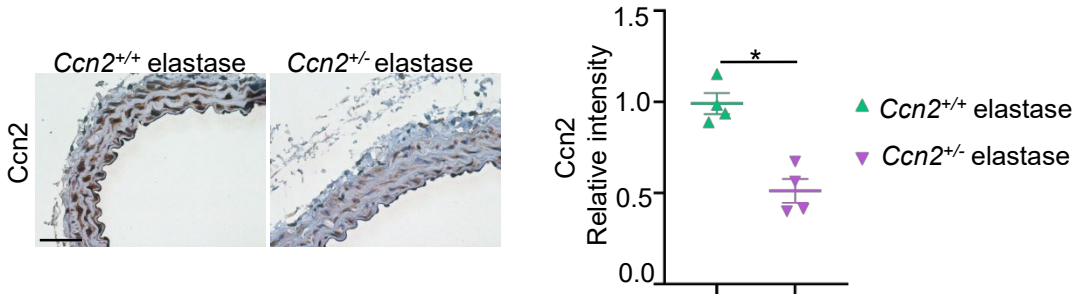

Figure S9. **CCN2 immunostaining in the aorta of elastase-induced mouse model of AAA as shown by IHC and its quantification.** Scale bar = 50 μm.